NUREG/CR-3938
EGG-2330

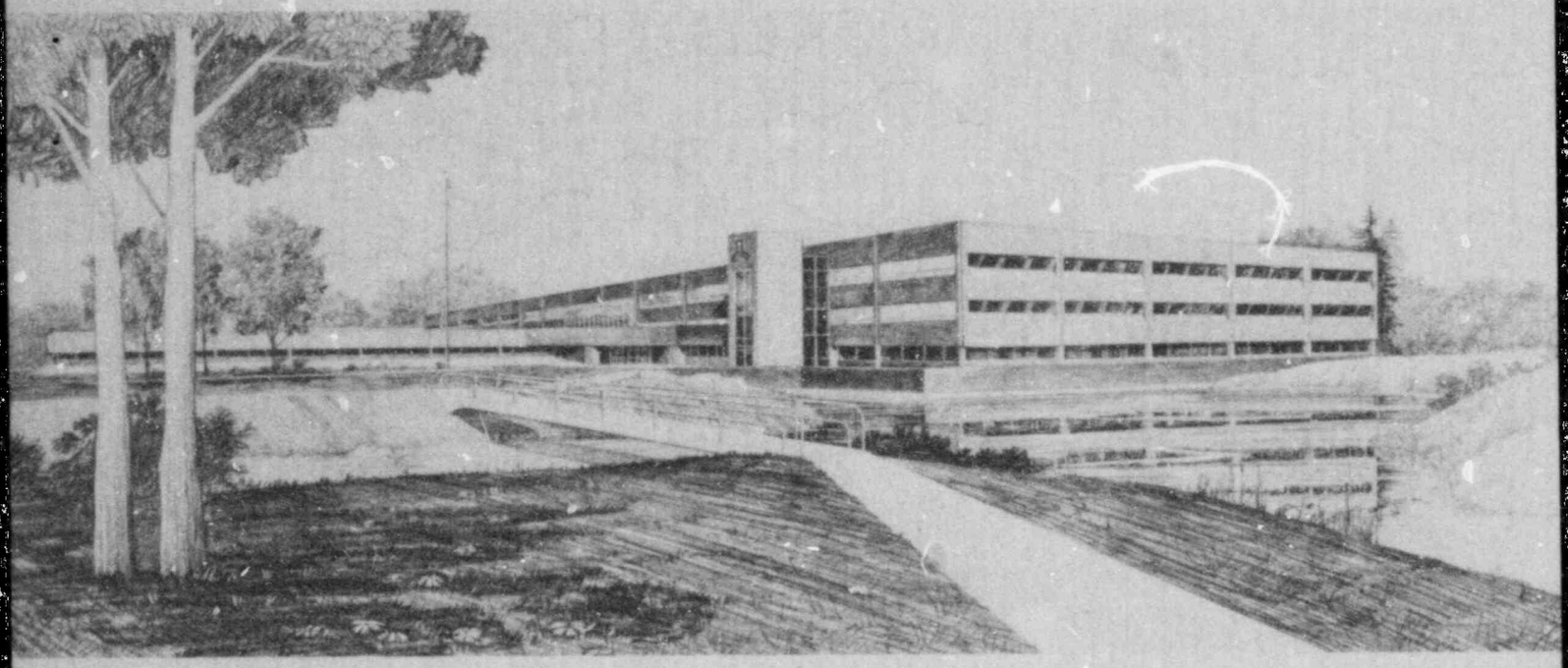

Idaho National Engineering Laboratory
Operated by the U.S. Department of Energy

Reactivity Initiated Accident Test Series Test RIA 1-4 Fuel Behavior Report

Beverly A. Cook
Zoel R. Martinson

September 1984

Prepared for the
U.S. Nuclear Regulatory Commission
Under DOE Contract No. DE-AC07-76IDO1570

EG&G Idaho

Available from

GPO Sales Program
Division of Technical Information and Document Control
U.S. Nuclear Regulatory Commission
Washington, D.C. 20555

and

National Technical Information Service
Springfield, Virginia 22161

NUREG/CR-3938
EGG-2336
Distribution Category: R3

REACTIVITY INITIATED ACCIDENT TEST SERIES TEST RIA 1-4 FUEL BEHAVIOR REPORT

Beverly A. Cook
Zoel R. Martinson

Published September 1984

EG&G Idaho, Inc.
Idaho Falls, Idaho 83415

Prepared for the
U.S. Nuclear Regulatory Commission
Washington, D.C. 20555
Under DOE Contract No. DE-AC07-76IDO1570
FIN No. A6305

ABSTRACT

This report presents and discusses results from the final test in the Reactivity Initiated Accident (RIA) Test Series, Test RIA 1-4, conducted in the Power Burst Facility (PBF) at the Idaho National Engineering Laboratory. Nine preirradiated fuel rods in a 3 x 3 bundle configuration were subjected to a power burst while at boiling water reactor hot-startup system conditions. The test resulted in estimated axial peak, radial average fuel enthalpies of 234 cal/g UO_2 on the center rod, 255 cal/g UO_2 on the side rods, and 277 cal/g UO_2 on the corner rods. Test RIA 1-4 was conducted to investigate fuel coolability and channel blockage within a bundle of preirradiated rods near the present enthalpy limit of 280 cal/g UO_2 established by the U.S. Nuclear Regulatory Commission. The test design and conduct are described, and the bundle and individual rod thermal and mechanical responses are evaluated. Conclusions from this final test and the entire PBF RIA Test Series are presented.

SUMMARY

The Reactivity Initiated Accident (RIA) Test RIA 1-4 was conducted in the Power Burst Facility (PBF) at the Idaho National Engineering Laboratory by EG&G Idaho, Inc. for the U.S. Nuclear Regulatory Commission (NRC). The objective of the test was to investigate coolability and channel blockage in a bundle of preirradiated fuel rods operated near the present NRC limit of 280 cal/g UO_2 radial average peak fuel enthalpy during an RIA event.

Nine fuel rods, preirradiated to a burnup of 5300 MWd/tU were tested in a 3 x 3 bundle configuration. The shortened pressurized water reactor (PWR) size test rods (0.914-m active fuel stack length) were not prototypical of boiling water reactor (BWR) fuel rods, but fuel rod behavior during an RIA was expected to be roughly equivalent for PWR and BWR rod types. Existing 3 x 3 bundle hardware was used, which resulted in a coolant flow area about 15% larger per rod than in a commercial BWR 8 x 8 bundle. Starting at BWR hot-startup conditions, the bundle was subjected to a single power transient, resulting in axial peak, radial average fuel enthalpies of 277, 255, and 234 cal/g UO_2 for the corner, side, and center rods, respectively.

Posttest examination revealed that all nine rods had failed, although the cladding was not fully oxidized and embrittled and there was no rod fragmentation. Because of fast flow recovery after the power burst, the cladding only oxidized locally. The cladding oxidation and failures occurred mostly on the sides of the rods facing the shroud walls. The cladding failures were characterized by high-strain-rate, brittle cracks and localized fuel and cladding melting. Brittle failure of thinned and totally oxidized cladding regions was not a major failure mechanism for the RIA 1-4 rods. Rod 804-5, the center rod, failed because of cladding melting when molten material from adjacent rods impinged upon it.

Test RIA 1-4 was the seventh test in the PBF RIA Test Series. The following questions were addressed by the test program:

- Will there be a loss of coolable core geometry when light water reactor (LWR) fuel is subjected to a radial average peak fuel enthalpy of 280 cal/g UO_2?
- Will energetic molten fuel-coolant interactions occur during a severe RIA and result in the production of a significant pressure pulse?
- What is the mechanism and threshold enthalpy for failure of LWR fuel during an RIA?

It was found, based on the PBF RIA test results, that subjecting a fuel rod to a radial average peak fuel enthalpy of 280 cal/g UO_2 may result in loss of coolable core geometry. Pressure pulse generation does not seem to be a significant safety concern during an RIA. The failure threshold for preirradiated fuel rods is as low as 140 cal/g UO_2 radial average peak fuel enthalpy, and the failure is due to high-strain-rate fracturing before the rod departs from nucleate boiling. Previously unirradiated rods fail at between 225 and 250 cal/g UO_2 by brittle fracture of thinned and totally oxidized cladding regions on quench.

ACKNOWLEDGMENTS

The authors extend their thanks to Robert D. McCormick for his contributions to this report.

CONTENTS

NOTE: All of the appendixes to this report are provided on microfiche attached to the inside of the back cover.

FIGURES

TABLES

REACTIVITY INITIATED ACCIDENT TEST SERIES TEST RIA 1-4 FUEL BEHAVIOR REPORT

INTRODUCTION

A major objective of the U.S. Nuclear Regulatory Commission's (NRC) Reactor Safety Research Program is understanding the performance of light water reactor (LWR) fuel under normal and accident conditions.[1-7] The reactivity initiated accident (RIA) has long been recognized as a potential source of nuclear fuel rod failure and reactor core damage, among the many possible accident conditions that may occur during LWR operation. To minimize the possibility of damage from postulated reactivity initiated accidents in commercial LWRs, NRC design requirements have been imposed on reactivity control systems to limit "the potential amount and rate of reactivity increase to assure that the effects of postulated reactivity accidents can neither (a) result in damage to the reactor coolant pressure boundary greater than limited local yielding nor (b) sufficiently disturb the core, its support structure, or other reactor pressure vessel internals to impair significantly the capability to cool the core."[5] NRC also requires that the number of fuel rods that will experience cladding failure during various RIAs be estimated and a conservative source term, subsequent transport of activity, and resulting doses to the public be calculated. In 1974, NRC established 280 cal/g UO_2 radially average peak fuel enthalpy as a limiting criterion for RIAs in light water reactors.

The axial peak, radial average fuel enthalpy limitation (<280 cal/g UO_2) is based on an NRC staff review of pre-1974 RIA fuel behavior data. The applicable RIA experimental data were obtained several years ago in the SPERT[a] (Capsule Driver Core) and TREAT[b] test programs, which investigated the behavior of single or small clusters of fuel rods during room temperature and atmospheric pressure conditions, no forced coolant flow, and zero initial power. Similar tests have been conducted in the Japanese Nuclear Safety Research Reactor.[8] The NRC staff review indicated that *failure consesquences were insignificant for total energy depositions* below 300 cal/g UO_2 for both previously irradiated and unirradiated UO_2 fuel rods subjected to rapid power excursions. Therefore, an *axial peak, radial average fuel enthalpy* of 280 cal/g UO_2 was considered a conservative maximum limit to ensure minimal core damage and maintenance of both short- and long-term core cooling capability.[a] The guidelines regarding reactor coolant pressure boundary stresses are assumed to be met if compliance with the enthalpy limitation is satisfactorily demonstrated. Additional calculations must be performed to prove that the guidelines regarding offsite dose consequences are met. Offsite dose consequences must be calculated assuming that (a) any pressurized water reactor (PWR) fuel rod that departs from nucleate boiling fails and (b) any boiling water reactor (BWR) rod subjected to a radial average peak fuel enthalpy of 170 cal/g UO_2 or above fails.

Compliance with the NRC licensing criteria is demonstrated by safety analyses performed by a reactor licensee or vendor. Results of the safety analyses must show the following:

1. "Reactivity excursions will not result in a radial average fuel enthalpy greater than 280 cal/g UO_2 at any axial location in any fuel rod,

2. Maximum reactor pressure during any portion of the assumed transient will be less than the value that will cause stresses to exceed the Emergency Condition stress limits as defined in Section III of the ASME Code,

3. Offsite dose consequences will be well within the guidelines of 10 CFR 100."[1]

a. Special Power Excursion Reactor Test.

b. Transient Reactor Test Facility.

a. Axial peak, radial average fuel enthalpy is less than the associated total energy deposition because of heat transfer from the fuel to the cladding and coolant during the power transients, and the relatively large fraction of the total energy that is due to delayed fissions (10 to 20%, depending on the reactor design).

An RIA test program was completed in the Power Burst Facility (PBF) at the Idaho National Engineering Laboratory (INEL) to provide RIA fuel behavior data under conditions more nearly typical of power reactor operation than in the previous SPERT and TREAT programs, thus allowing assessment of the NRC criteria. Seven RIA tests were conducted by the Thermal Fuels Behavior Program of EG&G Idaho, Inc. as part of the NRC Reactor Safety Research Program.[9,10] These tests have addressed the following key safety issues:

- Will there be a loss of coolable core geometry when LWR fuel is subjected to a radial average peak fuel enthalpy of 280 cal/g UO_2?

- Will energetic molten fuel-coolant interactions (vapor explosions) occur during a severe RIA and result in the production of a significant pressure pulse?

- What is the mechanism and threshold enthalpy for failure of LWR fuel during an RIA?

The seven PBF tests were all conducted with coolant conditions representative of hot-startup conditions for a BWR/6 reactor. The PBF RIA Series I tests are listed in Table 1.

The purpose of this report is to (a) present test results from the final RIA test (RIA 1-4) conducted at PBF to assess the consequences of fuel rod failure at fuel enthalpies near the NRC criterion of 280 cal/g UO_2 and (b) summarize the conclusions from the PBF RIA Test Series.

Expected Fuel Rod Behavior During an RIA

Fuel behavior during an RIA at hot-startup conditions can be separated into two time intervals during which different mechanisms dominate the fuel

Table 1. PBF RIA Series I Tests

Test	Fuel Rod Type	Fuel Enrichment (% U-235)	Burnup (MWd/tU)	Power Peaking Factor	Radial Average Total Energy Deposition (cal/g UO_2)	Radial Average Peak Fuel Enthalpy (cal/g UO_2)	Maximum Local[a] Fuel Enthalpy (cal/g UO_2)	Comments
RIA-ST-1 Burst 1	17 x 17 PWR	5.8	0	1.076	250	185	205	Did not fail; first test on RIA-ST-1 rod
RIA-ST-1 Burst 2	17 x 17 PWR	5.8	0	1.076	330	250	275	10% of fuel washed out; second test on RIA-ST-1 rod
RIA-ST-2	17 x 17 PWR	5.8	0	1.076	345	260	290	15% of fuel washed out
RIA-ST-3	17 x 17 PWR	5.8	0	1.076	300	225	250	Did not fail
RIA-ST-4	15 x 15 PWR	20	0	1.480	695	350[b]	530	Completely destroyed; pressure pulse of 35 MPa measured
RIA 1-1	Two Saxton	5.7	4600	1.130	365	285	330	Complete flow blockage
	Two Saxton	5.8	0	1.077	365	285	315	Severe failure; partial flow blockage
RIA 1-2	Four Saxton	5.7	5000	1.130	240	185	215	One rod failed; three rods did not fail
RIA 1-4	Nine Saxton	5.7	5300	1.130	295,270,245[c]	277,255,234[c]	340,300,265[c]	3 x 3 bundle; all failed

a. The maximum fuel enthalpy at the axial and radial peak locations.

b. The fuel enthalpy at the time of failure (~3 ms after the time of peak power).

c. Values for corner, side, and center fuel rods in bundle, respectively.

rod response.[11] During the first time interval, the fuel rod is thermally isolated from the surrounding coolant, and fuel heatup is the dominant mechanism that controls fuel rod response. During the second interval, the cladding temperature determines fuel rod response.

Initially the fuel rod power is essentially zero, but the fuel rod has a uniform radial average enthalpy of ~15 cal/g due to the 540 K temperature of the coolant and fuel. As the fuel rod is subjected to the power burst, it heats up and begins to expand thermally. Figure 1 shows representative temperature distributions in the fuel at various times during an RIA. The temperature distribution peaked near the fuel pellet surface in the fuel (shown in Figure 1) because of self-shielding of the fuel. The self-shielding results in a larger power density in the outer regions of the fuel pellet, causing higher fuel temperatures near the pellet surface. Some heat is transferred out of the pellet surface, resulting in a peak fuel temperature located just inside the fuel pellet surface. About 1% of the power burst energy is deposited in the cladding, resulting in a relatively low initial cladding heatup rate. The high fuel temperatures cause the fuel-cladding gap to close because of thermal expansion of the fuel. As the fuel-cladding gap closes, very large contact stresses are produced, resulting in either cladding failure due to high-strain-rate, brittle fracturing or tearing, or plastic deformation in the form of cladding thinning. The failures are characterized by angular fractures through the cladding wall. The cladding remains cold (600 K) during this phase and the strain rate determines if the cladding fails or plastically deforms.

If the internal rod pressure is lower than the coolant pressure, or the rod has already failed, the cladding deformation will be limited by the thermal expansion of the hot fuel. This radial deformation is about 1 to 3% in the axial peak region and is negative (i.e., collapses) at the cooler ends of the fuel rod. If the rod pressure is higher than the coolant pressure, relatively large strains are possible.

The fuel continues to heat up and, depending on the energy of the power burst, may begin melting. Because the peak fuel temperature occurs just inside the fuel surface, fuel melting may cause a rapid failure by melting the cladding. Peak fuel enthalpy occurs when the fuel rod begins transferring more heat out of the fuel than is produced by the delayed neutrons. Film boiling begins at approximately the same time that the peak fuel enthalpy occurs. The onset of film boiling terminates the time interval that fuel rod response is dominated by fuel heatup.

The cladding temperature becomes the dominant mechanism for fuel rod behavior during the second

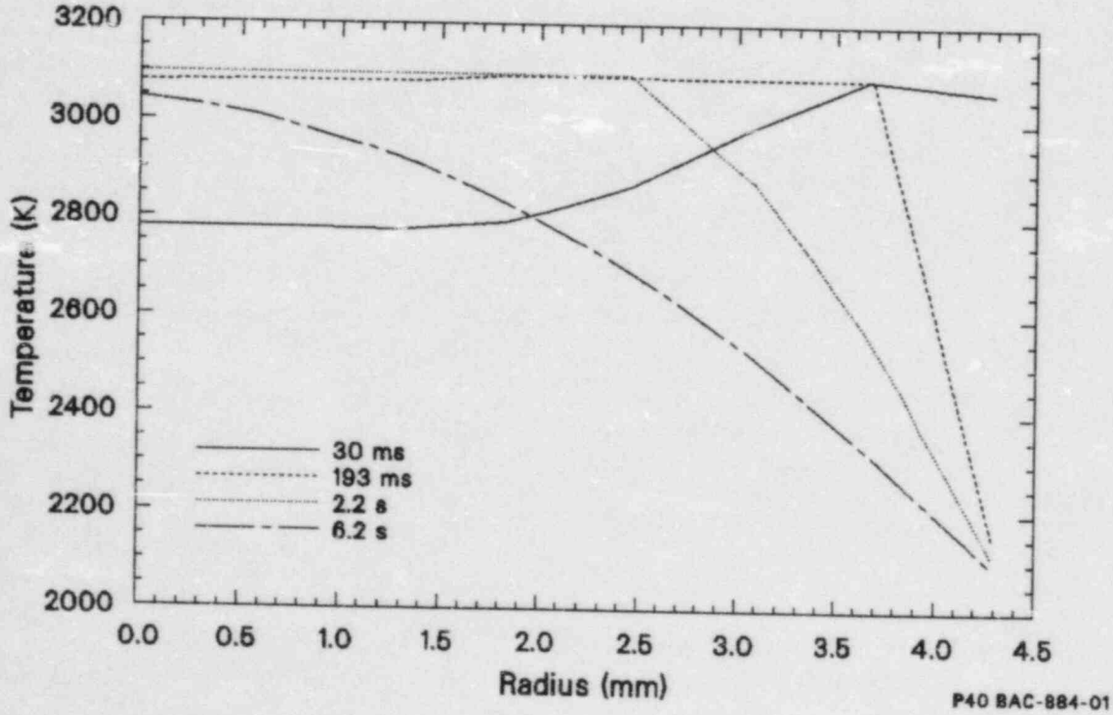

Figure 1. Temperature distributions in the fuel at various times during an RIA.

phase of the transient. The cladding is thermally isolated from the fuel until gap closure. After the gap closes, heat is transferred to the cladding, which acts as a heat sink while still relatively isolated from the coolant. The rod begins film boiling accompanied by cladding heatup when the heat produced in the fuel reaches the coolant. The high temperature of the cladding in a steam environment results in oxidation, thickening and thinning, and melting of the cladding.

The oxidation rate is maximum when the cladding reaches its peak temperature, about 1 to 3 s after the time of peak power. Cladding oxidation ends when the fuel rod rewets. The rewet time depends on the system hydraulics and varies between 3 and 25 s for the PBF tests. Rewet of the fuel rod terminates the RIA sequence but can cause fragmentation of the embrittled cladding and powdering of the fuel. The fragmentation of the fuel rod is important for assessing the postaccident heat transfer capability of the damaged fuel rod.

Review of PBF RIA Test Results

The seven tests in the PBF RIA series consisted of four scoping tests with previously unirradiated fuel rods and three tests using, for the most part, irradiated rods. The RIA Scoping Tests consisted of four separate, single-rod tests designated RIA-ST-1, RIA-ST-2, RIA-ST-3, and RIA-ST-4. Each test was conducted with a fuel rod assembled from unirradiated PWR zircaloy cladding and fuel (0.914-m active fuel length) enclosed in a cylindrical flow shroud. The four unirradiated test fuel rods were each subjected to one or more power transients, resulting in maximum axial peak, radial average fuel enthalpies ranging from 185 to 350 cal/g. The threshold for cladding failure of previously unirradiated fuel rods was between 225 and 250 cal/g UO_2 axial peak, radial average fuel enthalpy.[12]

The suspected scenario of cladding failure of previously unirradiated rods near the failure threshold began with plastic flow of the cladding, producing regions of cladding wall thickening and thinning. The zircaloy was then oxidized by steam and UO_2, and it became completely embrittled in the thinner regions. Extensive cracking of the embrittled cladding occurred because of thermal stresses during quench and rewet, following ~30 s of film boiling. Extensive fuel shattering along grain boundaries occurred in the two fuel rods tested at radial average peak fuel enthalpies of 250 and 260 cal/g, with up to 15% of the UO_2 fuel being flushed from the flow shrouds.

A coolant flow excursion out of the flow shroud, caused by rapid gamma and neutron heating of the coolant, has accompanied all of the RIA power bursts. Partial or total voiding of the flow shroud by such a coolant flow excursion may potentially influence the fuel-cladding heatup and failure.

Four individually shrouded, zircaloy-clad Saxton[a] fuel rods were tested in Test RIA 1-2. The rods were preirradiated to a burnup of ~5000 MWd/tU. Two rods were operated with internal pressures equal to BWR beginning-of-life conditions, and two rods were pressurized to reflect BWR end-of-life internal pressures. Starting at BWR hot-startup conditions, the rods were subjected to a power transient resulting in an axial peak, radial average fuel enthalpy of 185 cal/g UO_2.[13]

The rods reached cladding peak temperatures ranging from 1520 to 1700 K during the transient, with the high pressure rods reaching lower cladding peak temperatures than the low pressure rods. The failure in one of the low pressure rods consisted of 22 longitudinal cracks in the cladding. The cracking that occurred was similar to brittle failures observed due to pellet-cladding mechanical interaction. The other low pressure rod did not fail. The high pressure rods deformed slightly, with a maximum of 6.7% diametral strain and no rod failure. Some wall thinning occurred as a result of the increase in cladding diameter. There were no obvious differences between the two low pressure rods that would explain the failure of one rod and not the other. However, the low pressure rod that did not fail had been opened before the transient so a plenum pressure sensor could be installed. The other low pressure rod had not been opened following irradiation in the Saxton reactor.

Two previously irradiated (4600 MWd/tU) and two unirradiated fuel rods in separate flow shrouds were used in Test RIA 1-1.[14] All of the rods failed when subjected to a single power burst resulting in an axial peak, radial average fuel enthalpy of

a. A small, prototype PWR built by Westinghouse Electric Corp. and located in Saxton, Pa.

285 cal/g UO_2. The Test RIA 1-1 fuel rod behavior included severe cladding deformation, fuel and cladding melting, fuel swelling, and embrittled rod fragmentation. The primary consequences of these phenomena were loss of rod coolable geometry, dispersal of UO_2 to the coolant, and coolant flow blockages. Rapid thermal expansion of the fuel produced high-strain-rate failure of the cladding. Melting of the UO_2 produced relocation of fuel outside the cladding, from regions of severe deformation and rupture. However, the amount of relocation varied (e.g., greater relocation of molten fuel from the previously irradiated rods than the unirradiated rods) and was limited by solidification upon contact with solid fuel, cladding, or steam. Oxide on the surfaces of the cladding retained molten cladding material, further reducing fuel relocation by limiting dissolution of the UO_2 by molten zircaloy. Regions of cladding wall thinning were severely embrittled by oxidation and contributed to rod breakup and debris formation during quench. Rod fragmentation produced the largest volume of fuel relocation and dispersal to the coolant, leading to the coolant flow blockages and some fuel loss to the PBF test loop.

The mode of rod failure was strongly affected by prior irradiation. Fuel swelling induced by fission gas assisted in the rapid but localized relocation of molten fuel to the coolant and breakup of the fuel rod. Complete coolant flow blockages developed in the flow shrouds of the previously irradiated test rods within the first few seconds of the transient; however, only partial coolant flow blockages formed within the flow shrouds of the previously unirradiated test rods during the entire RIA transient. The differences in the time and extent of coolant flow blockages between the irradiated and unirradiated test rods were due to differences in the amount of molten fuel swelling and intermixing of molten fuel debris with solid fragments contributing to the flow blockages.

The cylindrical flow shrouds in Test RIA 1-1 are not representative of the coolant subchannel geometry in an LWR fuel bundle. Thus, coolant blockage behavior during a postulated RIA in a commercial LWR cannot be directly extrapolated from the shroud flow blockage behavior found in Test RIA 1-1. However, the rapid (~0.5 to 1 s) fuel dispersal to the coolant that occurred for the previously irradiated rods suggests that a potential exists for rapid loss of rod coolable geometry early in an RIA transient near the NRC limit of 280 cal/g. Therefore, Test RIA 1-4 was conducted to further investigate fuel coolability and channel blockage within a bundle of preirradiated fuel rods subjected to a peak fuel enthalpy of 280 cal/g.

Description of Test RIA 1-4

Test RIA 1-4 was composed of a 3 x 3 array (14.3-mm pitch) of fuel rods previously irradiated in the Saxton reactor to burnups of about 5300 MWd/tU. The rods were not opened prior to PBF testing. The fuel rod bundle was positioned within a zircaloy flow shroud by a series of four grid spacers centered at 15, 320, 625, and 930 mm above the bottom of the fuel region. A schematic of the fuel rods and flow shroud assembly is shown in Figure 2. Throughout this report, the fuel rods will be identified by the rod position numbers shown in Figure 2. Fuel Rods 804-1, 804-5, and 804-6 were each instrumented with two cladding surface thermocouples. The other six fuel rods were not instrumented. The axial elevations are measured from the bottom of the fuel stack. The coolant flow shroud had eight axial flux wires, two self-powered neutron detectors (SPNDs) and two self-powered gamma detectors (SPGDs). Test RIA 1-4 consisted of a nonnuclear loop heatup, a nuclear power calibration and preconditioning phase, a shutdown for replacement of Fuel Rod 804-2 with Rod 804-10 and flux wire replacement, a second loop heatup, and the power burst. A single power burst of about 50 ms in duration with a reactor period of 2.8 ms and a peak reactor power of 37,000 MW was conducted. The radial average peak fuel enthalpies attained in the corner, side, and center rods of the bundle were 277, 255, and 234 cal/g UO_2, respectively. Detailed descriptions of the test design and conduct are given in Appendixes A and B, respectively (all of the appendixes to this report are provided on microfiche attached to the inside of the back cover). On-line data for Test RIA 1-4 are presented in Appendix C.

This report presents an analysis, interpretation, and discussion of the results from Test RIA 1-4 and the PBF RIA test series in general. The "Fuel Rod Thermal and Mechanical Response" section includes the calculated fuel rod behavior and the bundle condition, bundle temperature distribution, cladding failure characterization, and fuel condition. Single rod and bundle test results, and the previously unirradiated and preirradiated fuel rod

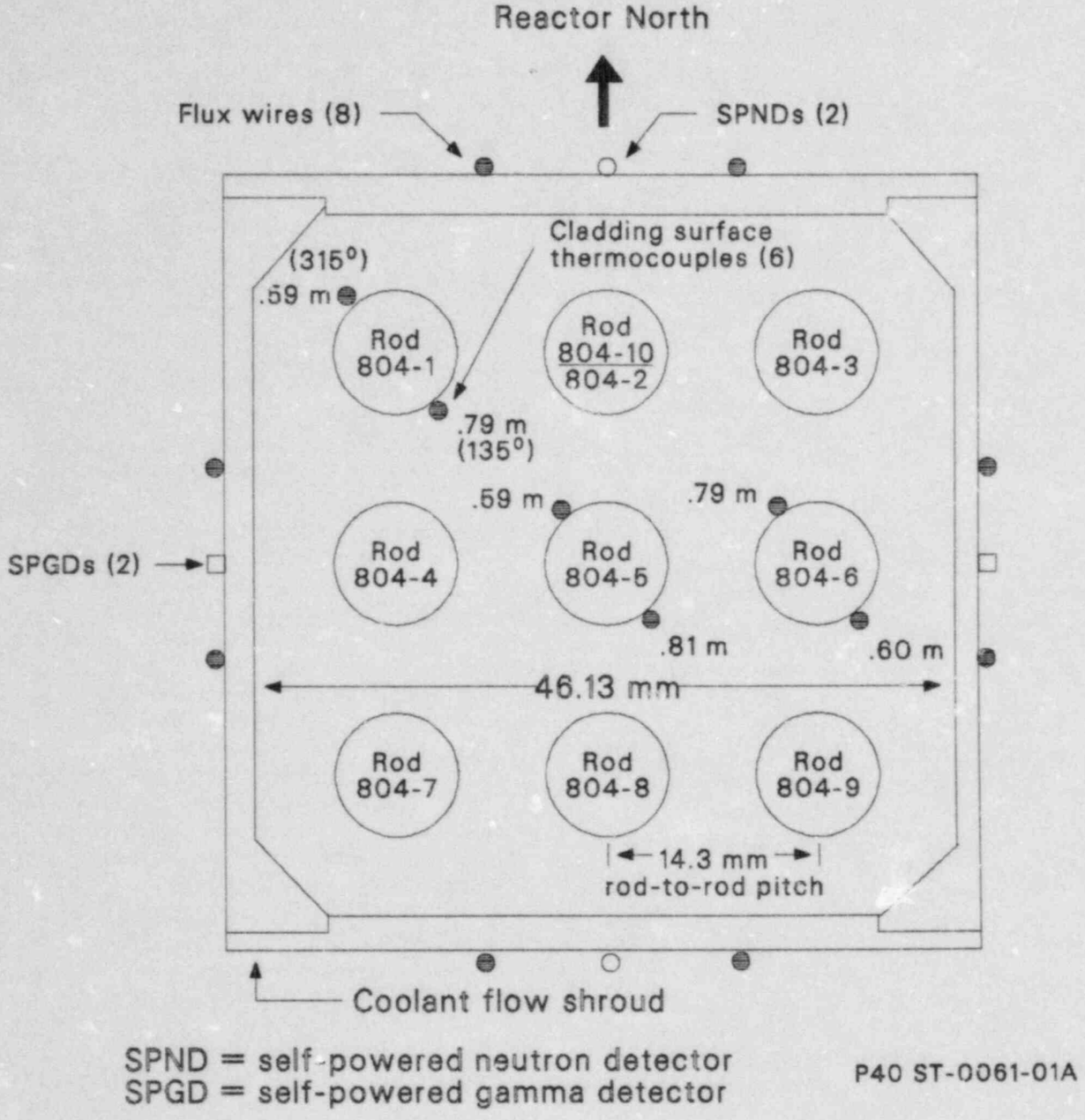

Figure 2. Schematic of RIA 1-4 fuel rods and flow shroud assembly with instrumentation.

test results are compared in the "Discussion" section. Conclusions involving reactor safety implications from the PBF RIA fuel behavior tests are presented in the "Conclusions" section. The measurements and calculations used to characterize the posttest condition and energy deposition of the test fuel rods are presented in Appendixes D, E, and F. Appendix G provides a description of documentation and computer tapes for Test RIA 1-4, and instructions for retrieving them.

FUEL ROD THERMAL AND MECHANICAL RESPONSE

Test RIA 1-4 was conducted to assess the consequences of fuel rod failure at a fuel enthalpy near the NRC criterion of 280 cal/g UO_2 in a nine-rod bundle. This section discusses the (a) predicted fuel rod behavior for the RIA 1-4 bundle as calculated for the specific test conditions and (b) overall bundle condition, bundle temperature distribution, and cladding and fuel condition determined from post-test examination.

Calculated Fuel Rod Behavior

Extremely rapid increases in fuel and cladding temperatures occur in short periods of time during a severe power burst. Although the magnitudes of the calculated fuel and cladding temperatures and associated stresses may not be entirely accurate, insight into the expected mechanisms of cladding and fuel rod damage can be obtained from a close inspection of the timing of the temperature increases, the temperature distributions, and the cladding strain rates. The Fuel Rod Analysis Program-Transient (FRAP-T6)[a] computer code was used to predict the transient behavior of the fuel rods during the RIA 1-4 power burst. The code calculates the variation with time of significant fuel rod parameters, including fuel and cladding temperature, cladding hoop stress and strain, cladding oxidation, and internal pressure. The measured coolant pressure, inlet coolant flow rate, and fuel rod power were input to FRAP-T6, together with pretest measured physical dimensions of the fuel rods and flow shroud. Details of the calculations are given in Appendix D.

The energy measurements, qualified on-line data, and reactor physics calculations used as input to FRAP-T6 are discussed in Appendixes B, C, and F, respectively. Figure 3 is a plot of the measured rod peak power, shroud inlet flow rate, and shroud coolant pressure during the first 0.6 s of the transient. A fuel rod peak power of 56 MW/m was reached during the power burst for the corner fuel rods. A sharp increase in the coolant pressure from 6.45 to 8.4 MPa occurred as a result of rapid heating of the coolant due to the extremely high neutron and gamma flux during the power burst. The rapid pressurization within the shroud expelled about 30% of the coolant from both ends of the

a. FRAP-T6, INEL Code Configuration Control No. F00404.

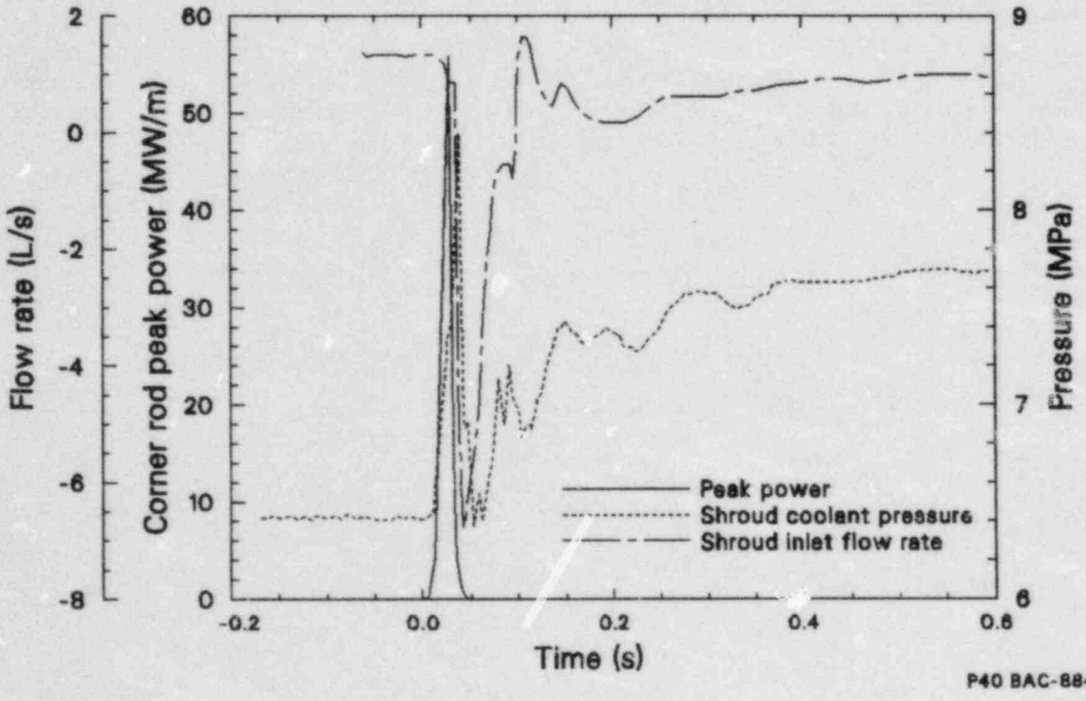

Figure 3. Measured corner rod peak power, shroud inlet flow rate, and shroud coolant pressure during the first 0.6 s after initiation of the RIA 1-4 power burst.

flow shroud. Normal upward flow through the shroud was restored within about 0.1 s as the coolant pressure decreased. The heat energy transferred from the test rods to the coolant produced a secondary gradual pressure increase to 7.7 MPa at 0.5 s due to bulk coolant boiling.

A summary of the results from the FRAP-T6 calculations for the corner, side, and center rods is given in Table 2. The calculated response for the side and center fuel rods is very similar to the response of the corner rods, and, therefore, only the corner rod response will be discussed in detail. Figure 4 presents the test rod power and the FRAP-T6 calculated cladding surface, fuel surface, fuel centerline, and peak fuel temperatures at the axial power peak during the first 300 ms after initiation of the power burst. The cladding surface, fuel surface, and fuel centerline temperatures during the first 25 s after initiation of the power burst are shown in Figure 5. The fuel temperatures rose very rapidly, with the peak fuel temperature (at a radial location near the fuel pellet outer surface) reaching the UO_2 melting point (3100 K) within 29 ms after initiation of the power burst. The radial average peak fuel enthalpy reached a maximum of 277 cal/g UO_2 at 42 ms after initiation of the power burst. A maximum of 73% of the pellet volume was calculated to be molten after 350 ms and remain molten for ~6 s. The fuel pellet surface temperatures reached an initial peak value of 2730 K at 28 ms (Figure 4), at which time the rod departed from nucleate boiling, and the cladding temperatures began to rise. The cladding reached the zircaloy melting point 18 ms later and remained molten for about 9 s. A 68-μm oxide layer and a 193-μm Xi layer[a] were predicted to form on the cladding outer surface at the peak axial power elevation of the corner rod.

a. The Xi layer is the combination of the oxide and oxygen-stabilized alpha zircaloy layers.

The rod power, fuel-cladding structural gap, and cladding hoop stress and hoop strain during the first 100 ms of the transient are shown in Figure 6. The rapid increase in fuel temperature while the cladding remains cool causes the fuel to expand faster than the cladding, resulting in closure of the fuel-cladding gap at the time of peak power. Pellet-to-cladding hard contact occurred at 25 ms and at a calculated fuel surface temperature of 2273 K. The hard pellet-cladding contact accounted for most of the initial heat transfer from the fuel during the burst. With the closing of the fuel-cladding gap, there is a rapid increase in cladding hoop stress up to a maximum of 517 MPa at 0.5 ms after peak power. The cladding hoop strain increased to a maximum of 2.6% at 15 ms after the time of peak power. A cladding failure probability of 89% due to cladding overstress is predicted by FRAP-T6 at 8.5 ms after peak power. The onset of cladding failure (probability >0) due to overstress begins at the time of peak power.

Observed Fuel Rod Behavior

After the test, the RIA 1-4 fuel rod bundle was examined both nondestructively and destructively, and the bundle condition was documented and analyzed. This section presents a description of the overall bundle condition, the bundle temperature distribution, a description of the cladding failures, and the fuel condition.

Bundle Condition. Photographs of each side of the bundle after disassembly are shown in Figure 7. Although all nine rods failed, the cladding was not fully oxidized and embrittled, and there was no rod fragmentation. Because of fast flow recovery after the power burst, only localized film boiling conditions prevailed for a short period of time, resulting in localized cladding oxidation. In general, the cladding oxidation and failures occurred mostly on the

Table 2. Summary of FRAP-T6 calculations for Test RIA 1-4

Rod Position	Radial Average Peak Fuel Enthalpy (cal/g UO_2)	Maximum Fuel Temperature (K)	Maximum Cladding Surface Temperature (K)	Maximum Fuel Stack Elongation (mm)	Maximum Cladding Elongation (mm)	Maximum Hoop Strain (%)	Maximum Hoop Stress (MPa)	Cladding Failure Probability Due to Overstress (%)
Corner	277	3141	2098	26.2	6.9	2.6	517	89
Side	255	3098	2098	25.4	6.0	2.0	515	9
Center	234	3096	2098	24.3	6.4	1.7	498	7

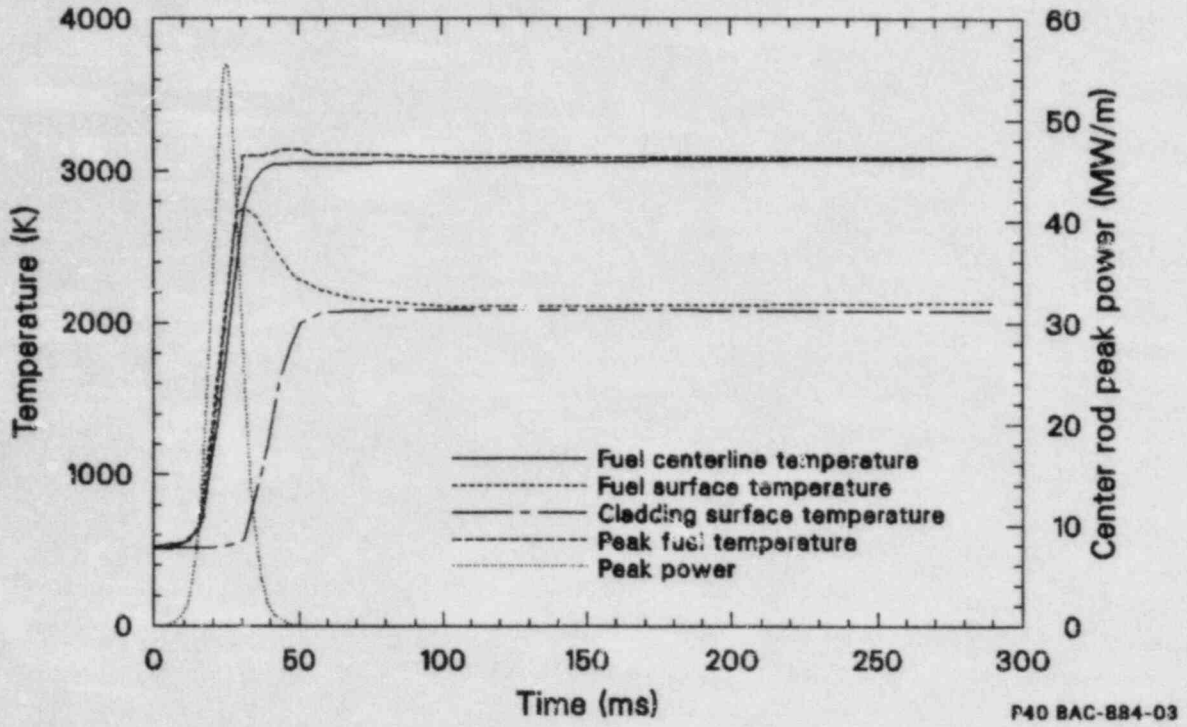

Figure 4. Corner rod peak power and FRAP-T6 calculated fuel and cladding temperatures during the first 300 ms after initiation of the RIA 1-4 power burst.

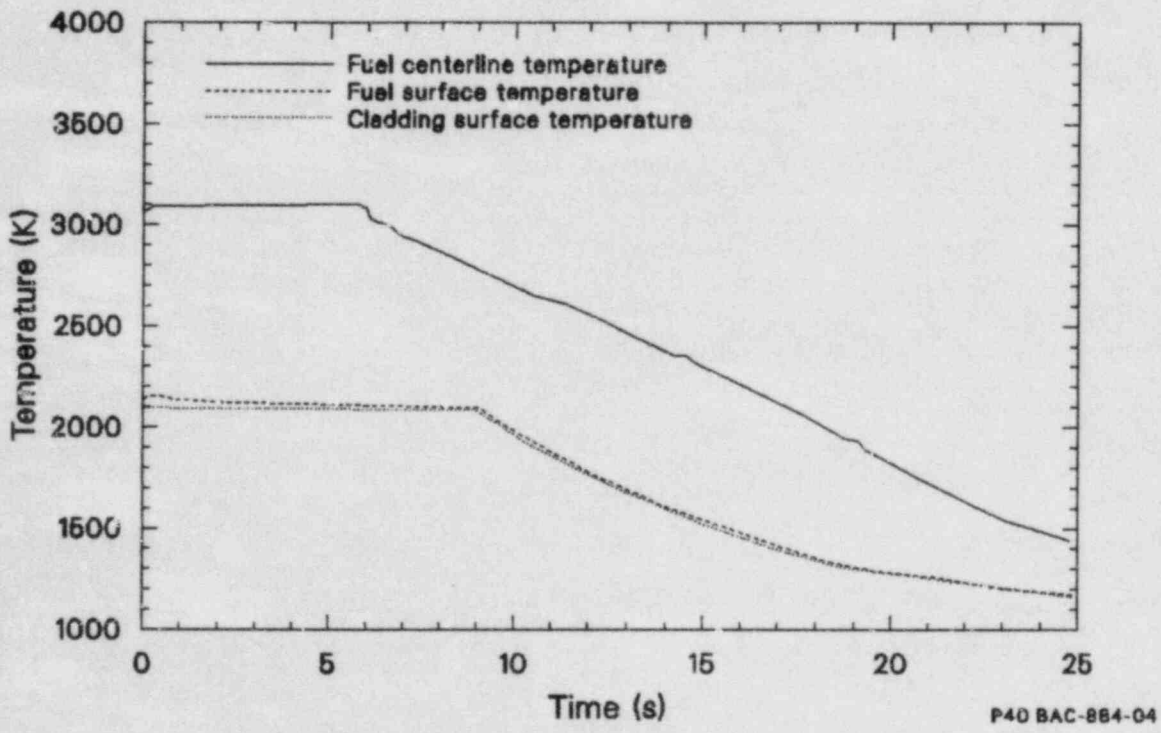

Figure 5. FRAP-T6 calculated fuel and cladding temperatures during the first 25 s after initiation of the RIA 1-4 power burst.

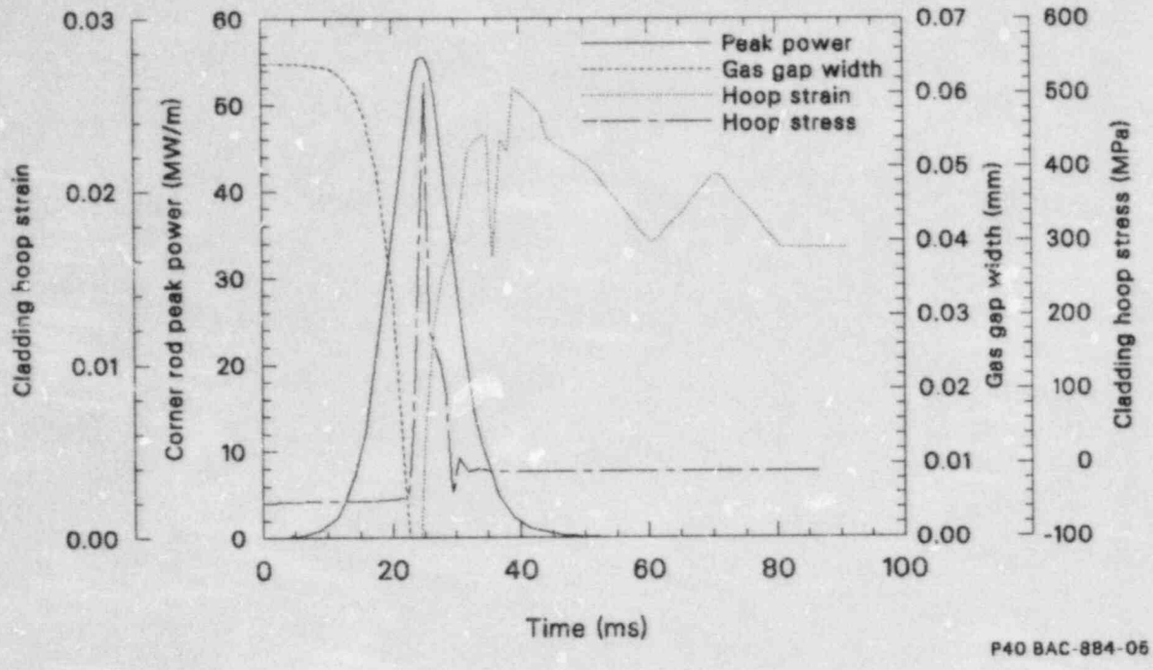

Figure 6. Corner rod peak power and FRAP-T6 calculated pellet-to-cladding gap width, cladding hoop strain, and cladding hoop stress during the first 100 ms of the RIA 1-4 power burst.

sides of the rods facing the shroud walls. There are many heat affected regions on the inside of the west shroud wall, where molten material from Rods 804-1, -4, and -7 contacted the shroud wall (Figure 8). The west side of the bundle (Figure 7) shows failures in all three rods at the 47.5-cm elevation.

There appears to be material connecting Rods 804-8 and 804-9 at the 47.5-cm elevation, as viewed from the south side of the bundle. When the bundle was disassembled, it was discovered that Rod 804-8 was stuck to Rod 804-5 at this elevation. Figure 9 shows the materials from Rods 804-8 and 804-9 on Rod 804-5. Apparently, molten material from Rod 804-9 impinged on Rods 804-8 and 804-5, causing failures at the same elevation in those two rods. All of the failures of Rod 804-8 were on the sides facing Rods 804-9 and 804-5. The view of the east side of the bundle (Figure 7) shows material from Rod 804-3 impinging on Rod 804-6 at the 53.5-cm elevation.

Bundle Temperature Distribution. Cladding peak temperatures were estimated for several elevations of each rod by examining the cladding microstructure. The four broad temperature ranges that can be characterized by microstructural changes are (a) as-fabricated, stress relieved zircaloy at $T < 920$ K; (b) equiaxed alpha zircaloy at $920 < T < 1105$ K; (c) two-phase mixture of alpha and beta zircaloy at $1105 < T < 1245$; and (d) beta zircaloy at $1245 < T <$ T melting (2125 K for beta phase and 2245 K for oxygen-stabilized alpha phase). A fifth criterion for determining cladding peak temperature from microstructure relates to phase changes in the ZrO_2 with temperature. Below about 1850 K, beta-phase zirconium (zircaloy) reacts with oxygen to form a layer of ZrO_2 (tetragonal form) and oxygen-stabilized alpha zircaloy [α(O)Zr]. When quenched to ambient temperatures, the tetragonal form transforms to a monoclinic structure (the stable form of ZrO_2). Above 1850 K, the beta-phase zircaloy reacts to form a layer of cubic ZrO_2 adjacent to the growing layer of α(O)Zr. Quenching produces a monotectoid decomposition of the oxide, reducing the cubic form to tetragonal oxide and alpha zircaloy. The tetragonal oxide transforms to the monoclinic form during quenching to ambient temperatures. The room temperature microstructure of the monotectoid material is characterized by alpha-phase zircaloy appearing as a second phase within the monoclinic ZrO_2. The cladding peak temperatures based on the various microstructures are presented in Table 3.

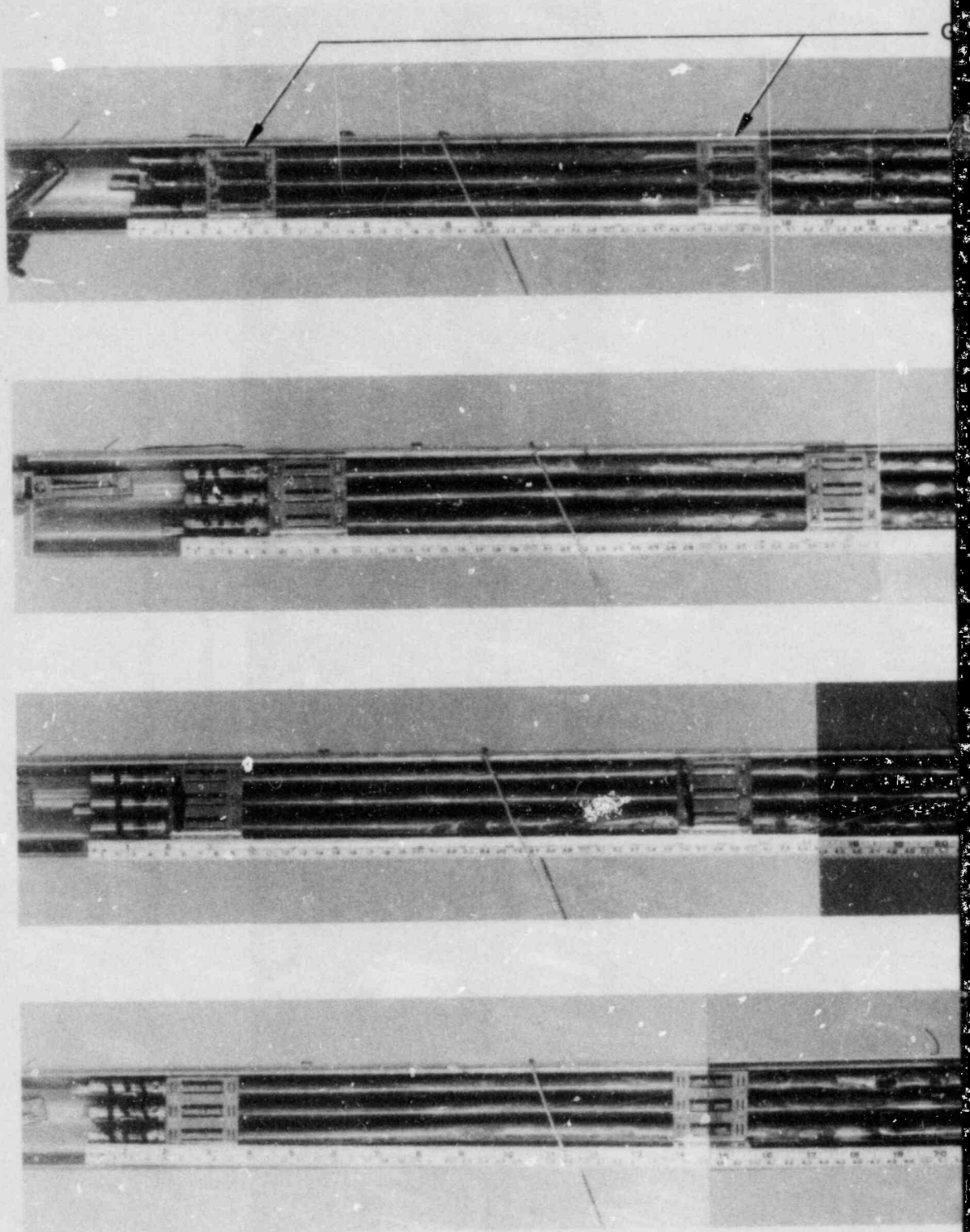

Bottom

Figure 7. Overall

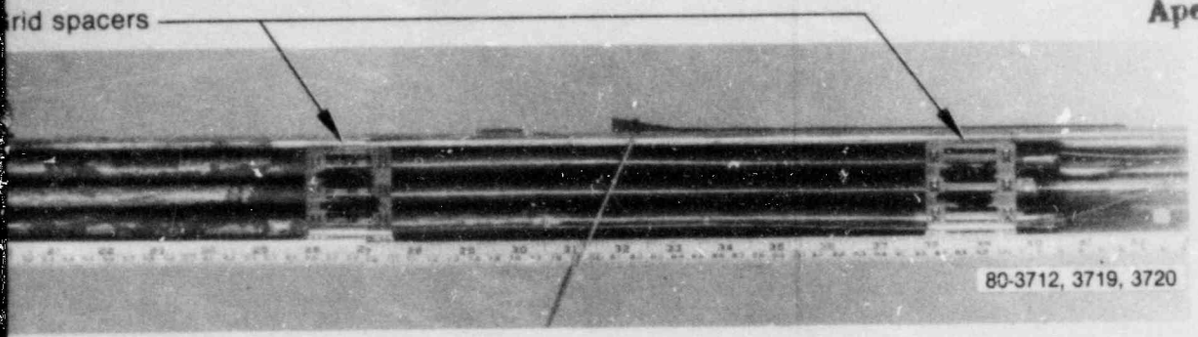

a. North view.

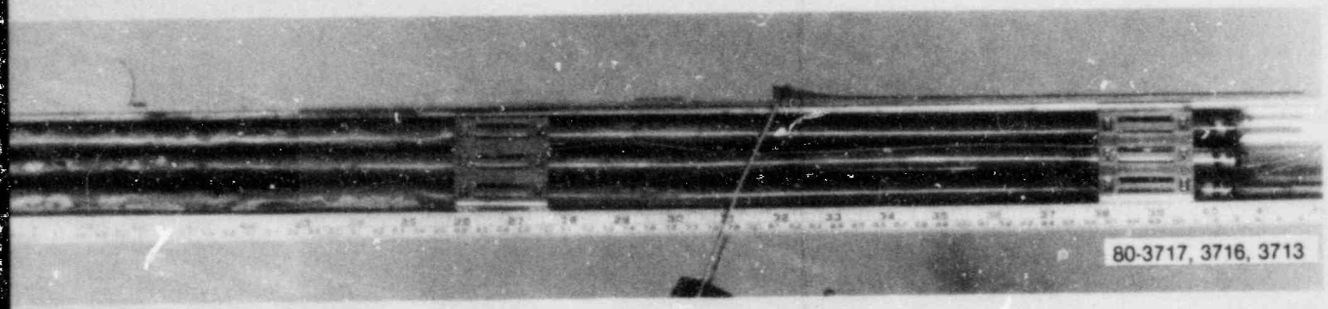

b. East view.

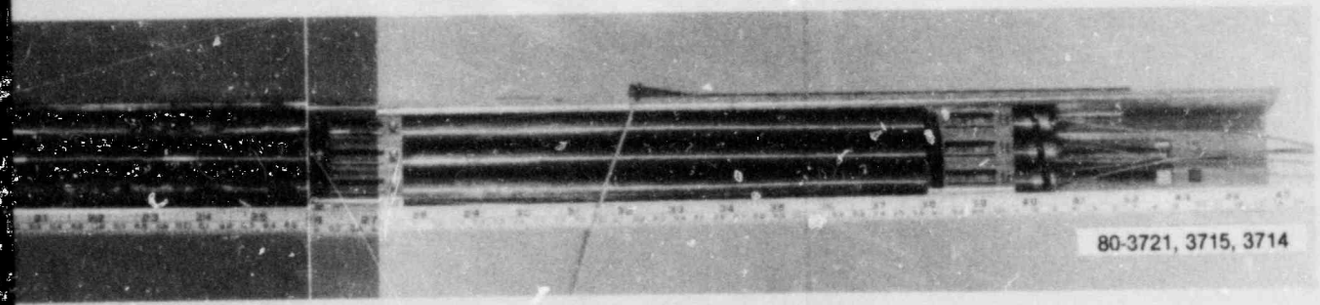

c. South view.

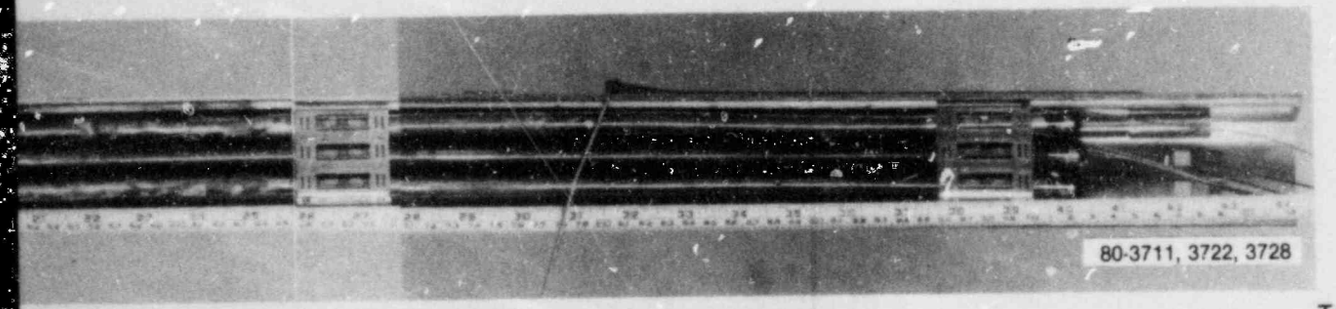

d. West view.

Top

iew of the RIA 1-4 bundle after the test.

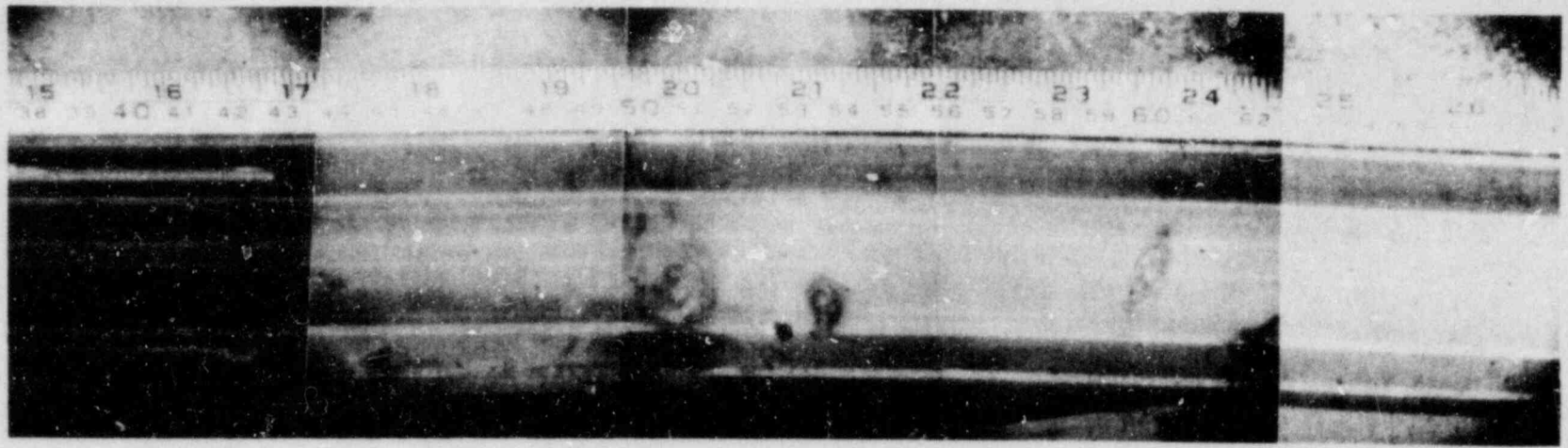

Figure 8. Heat affected region on the inside of the west shroud wall.

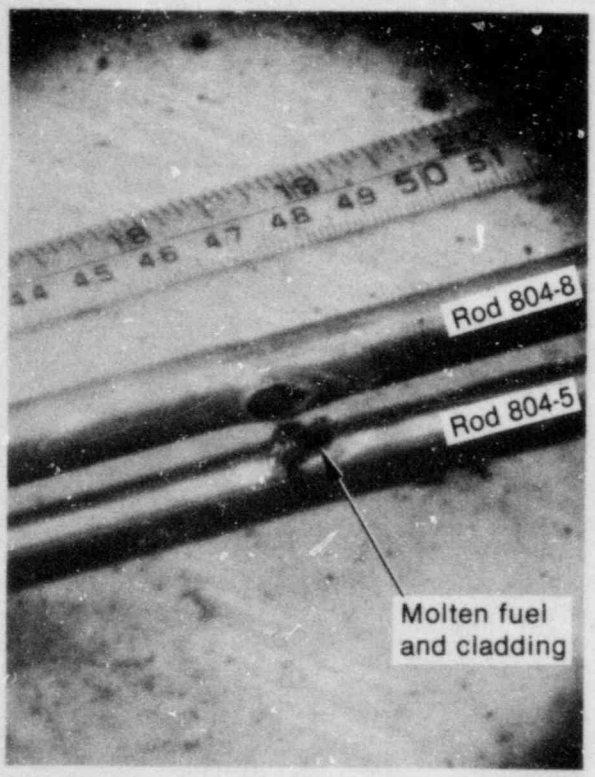

Figure 9. Previously molten materials from Rods 804-8 and 804-9 on Rod 804-5.

The COBILD[a] computer code was used to estimate the peak cladding surface temperatures from the measured oxide thicknesses. The oxide and α(O)Zr layer thicknesses were calculated using a parabolic rate equation. The code requires a temperature-time history to be input and varies the magnitude of the profile until the measured layer thicknesses are obtained. The cladding thermocouple temperature profiles were input to COBILD. The thermocouple at the 0.59 m elevation of Rod 804-6 was used for all elevations on all of the side rods, the thermocouple at 0.59 m of Rod 804-1 was used for all elevations on all corner rods, and the thermocouple at 0.59 m of Rod 804-5 was used for all elevations of Rod 804-5. The estimated uncertainty in temperature of ± 80 K is due to photographic magnification and measurement uncertainties of the oxide and α(O)Zr layers. The calculated temperatures are listed in Table 3.

Using the thermocouple profiles may lead to errors in the calculated cladding temperatures. The cladding surface thermocouples have been observed to quench early, thereby shortening the apparent time at temperature of the cladding. An incorrect time at temperature (specifically, a shorter time at temperature) would lead to a higher calculated cladding peak temperature for given ZrO_2 and α(O)Zr layers. By comparing the COBILD calculated peak temperatures with the temperature ranges from the observed microstructures, the calculated temperatures appear to be high, indicating that the thermocouples probably quenched before the cladding. The highest reasonable cladding temperatures are presented in Table 3 under the column labeled "Best-Estimate Cladding Peak Temperature." Some of the highest cladding temperature estimates were reduced to match those from the observed microstructures. Cladding peak temperatures that fell within the limits set by the observed microstructures were not adjusted.

Eight of the nine rods subject to the transient had cladding failures at ~0.42 m, and samples were cut at this elevation for metallographic examination. The cladding peak temperature should be highest on the side of the rod facing the shroud because of self-shielding effects. However, in many locations, high-strain-rate failures occurred early in the transient, before the cladding reached peak temperature and the fuel attained its maximum thermal expansion. When the fuel continued to expand after cladding failure, the cladding may have deformed away from the fuel surface and may not necessarily have been in close contact with the fuel at the orientation where the fuel surface temperature was the hottest. The orientation of failure is listed in Table 3 for each elevation examined. When the failure was a high-strain-rate failure, the highest cladding peak temperature was oriented 180 degrees from the failure. When the failure was characterized by fuel and cladding melting, the highest cladding peak temperature occurred at the orientation of the failure.

Characterization of Cladding Failures. All of the fuel and cladding failure mechanisms that occurred during the RIA single-rod tests in PBF also occurred during the RIA 1-4 test. However, the extent and severity of damage of the RIA 1-4 rods was less than expected, based on the results of the single-rod tests. The general types of rod deformation and failures observed are (a) high-strain-rate failures, (b) cladding plastic deformation and melting, and (c) brittle failure of highly oxidized cladding. The locations and orientations of all rod failures for Test RIA 1-4 are listed in Table 4.

a. The COBILD code is described in Appendix F of Reference 13.

Table 3. Cladding peak temperature estimates for Test RIA 1-4

(Rod) Sample	Elevation (m)	Orientation (degrees)	Temperature from Microstructure (K)	Temperature from COBILD[a] (K)	Best-Estimate Cladding Peak Temperature (K)	Orientation of Failure (degrees)
(804-1)						
M-12	0.312	80	1250 < T < 1850	1870	1850	270
		170	1250 < T < 1850	1902	1850	
		250	1250 < T < 1850	1934	1850	
		260	1250 < T < 1850	1775	1775	
M-13	0.416	90	1250 < T < 1850	1965	1850	270
		180	1850 < T < 2100	2124	2100	
		240	1850 < T < 2100	2156	2100	
M-13	0.419	0	1250 < T < 1850	1997	1850	270
		190	1850 < T < 2100	2029	2029	
M-14	0.503	35	1850 < T < 2100	2282	2100	250
		90	∿1850	2029	1850	
		180	∿1850	1997	1850	
		270	1850 < T < 2100	2219	2100	
M-15	0.578	45	1250 < T < 1850	2061	1850	270
		135	1250 < T < 1850	1870	1850	
		260	1250 < T < 1850	1965	1850	
		270	∿1850	1965	1850	
		325	1250 < T < 1850	1934	1850	
(804-4)						
M-43	0.409	0	1250 < T < 1850	1938	1850	290
		90	1250 < T < 1850	1938	1850	
		180	1250 < T < 1850	1863	1850	
		270	1250 < T < 1850	1639	1639	
(804-5)						
M-51	0.416	0	1250 < T < 1850	1790	1790	160
		120	1250 < T < 1850	1641	1641	
		240	1250 < T < 1850	1716	1716	
(804-6)						
M-61	0.358	0	1250 < T < 1850	1838	1838	90
		90	1850 < T < 2100	2037	2037	
		180	1250 < T < 1850	1714	1714	
		270	1250 < T < 1850	1838	1838	
M-63	0.421	0	1250 < T < 1850	1689	1689	90
		90	1850 < T < 2100	2161	2100	
		180	1250 < T < 1850	1689	1689	
		270	1250 < T < 1850	1714	1714	

Table 3. (continued)

(Rod) Sample	Elevation (m)	Orientation (degrees)	Temperature from Microstructure (K)	Temperature from COBILD[a] (K)	Best-Estimate Cladding Peak Temperature (K)	Orientation of Failure (degrees)
M-64	0.484	45	1850 < T < 2100	1863	1863	45
		150	1250 < T < 1850	1863	1850	
		220	1250 < T < 1850	1813	1813	
		330	1250 < T < 1850	1639	1639	
(804-7)						
M-73	0.417	10	1250 < T < 1850	1744	1744	290
		90	1250 < T < 1850	1839	1839	
		150	1250 < T < 1850	1775	1775	
		210	1250 < T < 1850	1712	1712	
		300	1250 < T < 1850	1712	1712	
(804-8)						
M-82	0.428	50	1250 < T < 1850	1838	1838	90
		110	1250 < T < 1850	1664	1664	
		170	1250 < T < 1850	1565	1565	
		230	1250 < T < 1850	1565	1565	
		290	1250 < T < 1850	1664	1664	
		320	1250 < T < 1850	2012	1850	
(804-9)						
M-94	0.421	0	1250 < T < 1850	1712	1712	270
		90	1250 < T < 1850	1902	1850	
		180	1250 < T < 1850	1965	1850	
		280	1250 < T < 1850	1521	1521	
(804-10)						
M-2	0.426	80	1250 < T < 1850	1714	1714	0
		170	—	1813	—	
		260	—	1913	—	
		330	1850 < T < 2100	2211	2100	
M-3	0.448	45	1850 < T < 2100	2161	2100	0
		90	1250 < T < 1850	1863	1850	
		180	1250 < T < 1850	1639	1639	
		270	1250 < T < 1850	1788	1788	
M-3	0.445	45	1850 < T < 2100	2012	2012	0
		100	1250 < T < 1850	1589	1589	
		180	1250 < T < 1850	1739	1739	
		270	1250 < T < 1850	1863	1850	

a. The estimated uncertainty of these temperatures is ±80 K.

Table 4. Locations of rod failures for Test RIA 1-4

Rod	Elevation of Failure (m)	Orientation of Failure (degrees)
804-1	0.32	270
	0.37	30
	0.42	270
	0.45	270
	0.51	250
	0.53	0
	0.59	270
804-3	0.28	90
	0.33	170
	0.48	130
804-4	0.41	290
	0.43	290
804-5	0.34	90
	0.43	160
804-6	0.35	90
	0.39	90
	0.42	90
	0.45	90
	0.48	45
804-7	0.42	290
	0.54	190
804-8	0.34	10
	0.43	90
	0.52	100
	0.53	100
804-9	0.34	100
	0.36	100
	0.42	270
	0.50	100
	0.52	110
	0.56	110
804-10	0.42	0
	0.44	0

Multiaxial stresses at high strain rates are produced in zircaloy cladding during RIAs by the thermally expanding fuel. The cladding is expected to fail in regions where local stresses exceed the ultimate strength. The mechanical anisotropy of typical LWR cladding at low temperature (at the $\alpha + \beta$ two-phase zircaloy region and lower) limits the ability of the cladding to accommodate the radial and tangential expansion of the fuel by cladding radial wall thinning. The higher the strain rates imposed on the cladding, the higher the temperature required to achieve significant cladding strain without failure. The high-strain-rate failures observed in the RIA tests are characterized by through-wall fractures exhibiting fracture angles of roughly 35 and 57 degrees. Those fracture angles are close to the angles associated with the tensile {1121} <1126> and compressive {1011} <1012>[a] twinning modes operative in zircaloy at low (~1140 K) cladding temperatures. The twinning modes require a higher initiating stress than either prismatic or basal slip; however, the cladding texture in the test rods indicates that deformation by prismatic or basal slip is unfavorable. Sufficient stress is present with the very high strain rates produced by the rapid thermal expansion of the fuel during the RIA transient to make twinning deformation modes significant.[14]

Examples of the high-strain-rate failures are shown in Figure 10. A higher magnification photograph of one of the failures is shown in Figure 11. The thicknesses of the oxygen-stabilized alpha and oxide layers on the fracture surfaces are equal to the thicknesses of the layers on the outside surface of the cladding, indicating that the failures occurred before initiation of film boiling. Additional thermal expansion of the fuel after cladding rupture plus fission product induced swelling of the fuel resulted in opening of the cracks.

When the ultimate stress is exceeded at a higher cladding temperature or lower strain rate, some plastic deformation of the cladding occurs. Although the fracture shown in Figure 12 is similar to the high-strain-rate failures shown in the previous figures, there is some deformation of the fracture tip.

At even higher cladding temperatures, near the zircaloy melting point, significant wall thickening and thinning occurs without through-wall failures.

a. Standard Miller Indices notation for crystallographic directions and planes.

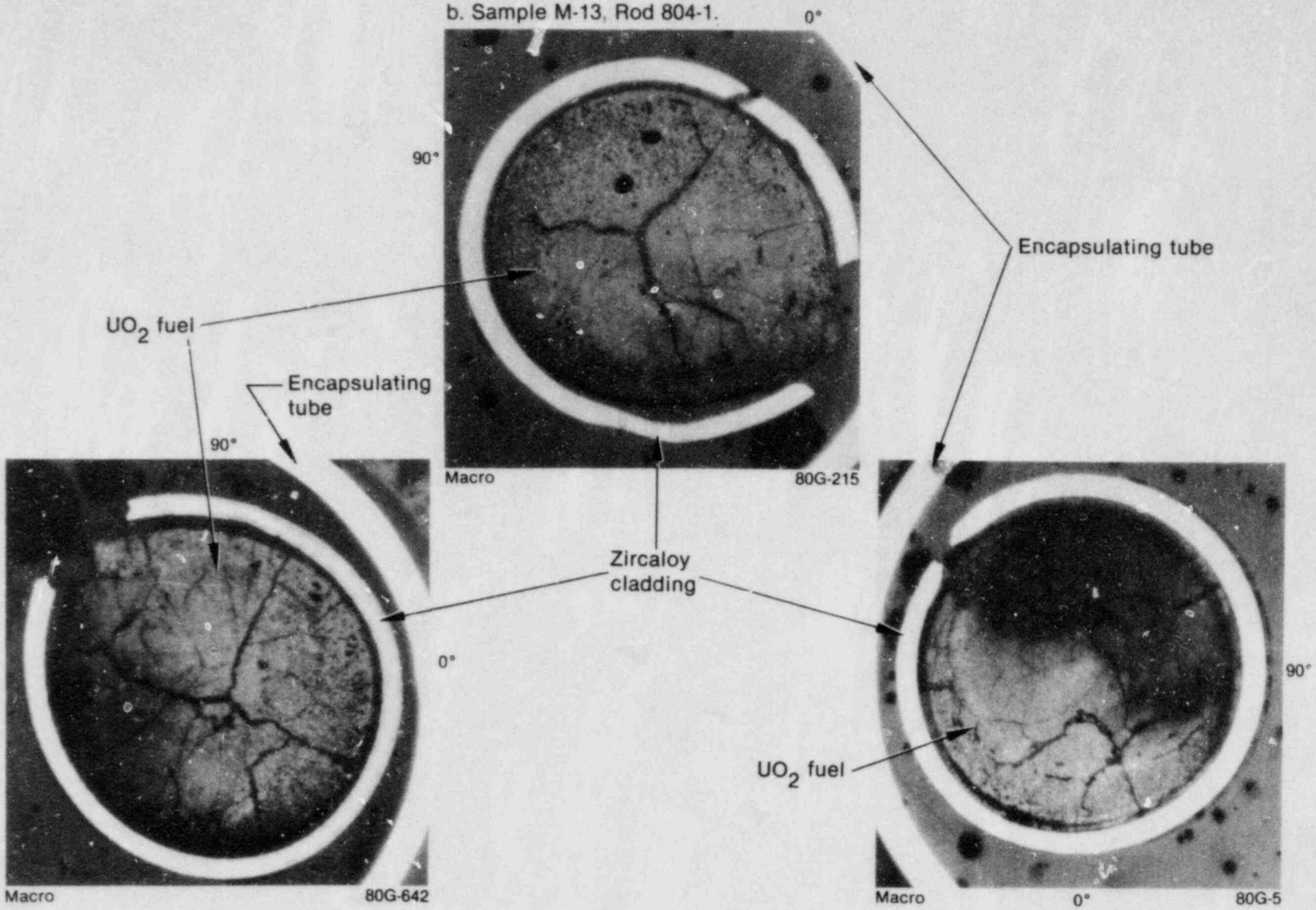

Figure 10. High-strain-rate failures at three cross sections of the RIA 1-4 rods.

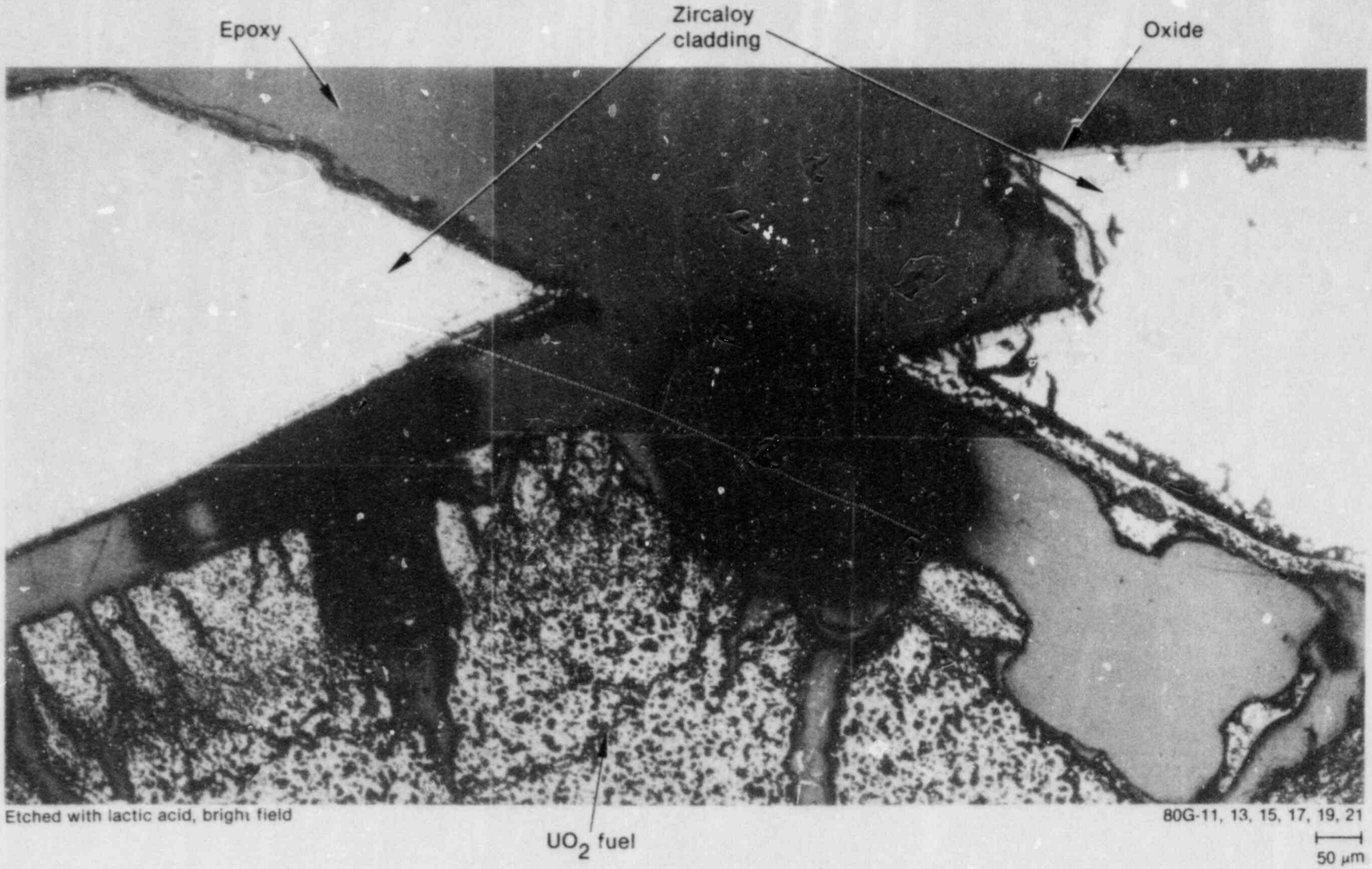

Figure 11. High-strain-rate failure from Rod 804-1.

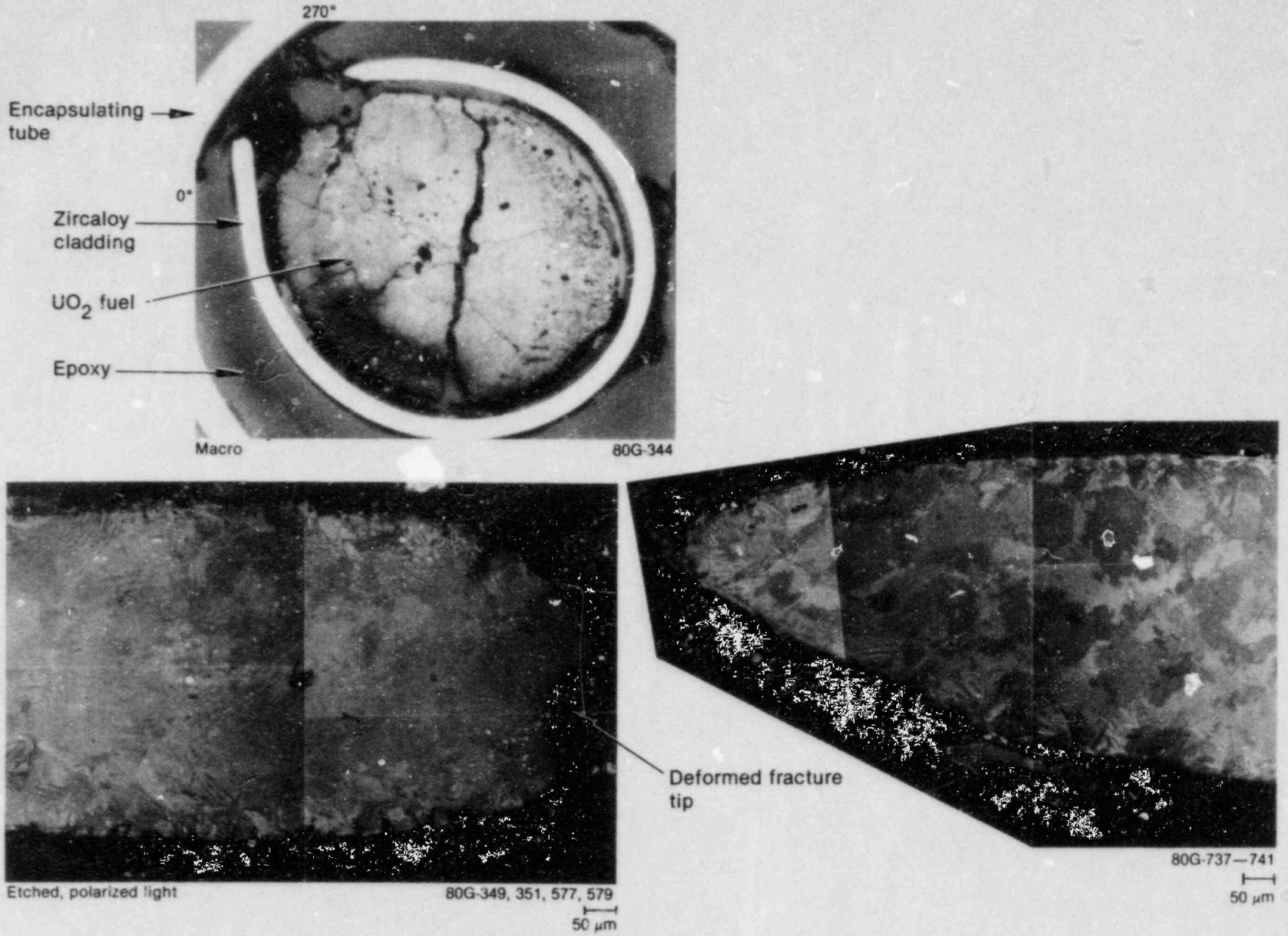

Figure 12. Failure from Rod 804-7 showing some plastic deformation.

Incipient cracks may be observed on the inside surface of the cladding at these areas. Brittle failure of the cladding can occur at the thinned regions on quench if the cladding experienced film boiling after the deformation occurred and became heavily oxidized at the thinned sections. Two photographs of cladding with wall thinning are shown in Figure 13. There are brittle failures at the thin-wall regions at other locations, but this was not a major failure mechanism for the RIA 1-4 rods.

Limited melting of the cladding can occur when the fuel surface temperature exceeds the melting temperature of the cladding. Melting was observed (Figures 14 and 15) at the fracture tips of some of the high-strain-rate failures. The temperature of the fuel rose high enough during the power transient that melting of the cladding occurred after the high-strain-rate failure. In both cases, the molten zircaloy relocated to the outside surface of the cladding and is still attached by means of the outside surface ZrO_2 layer, which probably did not melt but became very plastic.

At higher peak fuel temperatures, pockets of molten fuel form near the outside surface of the fuel pellets. Figures 16, 17, and 18 all show molten fuel interaction with cladding. In Figure 16, the cladding first failed by high-strain-rate failure, as evidenced by the ZrO_2 layer on the fracture surface on one side of the failure. Subsequently, localized fuel and cladding melting and interaction occurred. A significant amount of material is missing at this elevation and must have flowed to other elevations after melting.

Fission gases form bubbles in the fuel during heating and especially during melting. When the molten fuel intermixes with the molten cladding, a highly porous, frothy mixture can be produced (Figure 17). At the elevation shown in Figure 18, the molten mixture was contained by an oxide layer, probably mostly ZrO_2. It is likely that the excess material shown in Figure 18 flowed down from the outside surface of the cladding and solidified at this elevation, with an oxide forming around the outside of the drop.

Fuel Condition. Several time-temperature dependent fuel phenomena were observed in the RIA 1-4 fuel rods that affect fuel rod performance and, specifically, rod failure. This section discusses fuel temperature, fission gas movement, bubble formation and fuel swelling, grain boundary shattering, grain growth, fuel melting, and fuel oxidation for various radial nodes in the fuel pellets.

Fuel Temperature Profile. In an RIA transient, the time-temperature profile for each axial and radial position in the fuel is different. During the RIA transient, the fuel heats up much faster than the cladding, and the fuel peak temperature is initially located near the fuel surface. The calculated radial temperature distribution across the fuel at the peak flux location at times between 30 ms and 6.2 s is shown in Figure 1. The fuel centerline, fuel surface, and cladding surface temperatures for the first 25 s of the transient (as calculated by FRAP-T6 for the RIA 1-4 test conditions) are shown in Figure 5. The highest temperature fuel region, near the pellet surface, reached a peak temperature at 30 ms into the transient. The fuel temperature at the pellet surface stayed above 2500 K for only 14 ms (Figure 4). Table 5 shows the fuel radial nodes used in the FRAP-T6 calculation, the time the peak temperature was reached, and the total time above 2500 K for the peak power elevation. The center of the pellet remained above 2500 K for over 13 s.

The calculated temperatures are somewhat high as compared with those indicated by observed microstructures. The FRAP-T6 calculations indicated that the whole pellet at the peak power

Table 5. FRAP-T6 calculated time at peak fuel temperature

Node	Radial Position (mm)	Time of Peak Temperature (s)	Total time Above 2500 K (s)
1	0.00	0.351	13.174
2	0.61	0.351	13.174
3	1.23	0.311	12.174
4	1.84	0.217	11.174
5	2.54	0.036	10.174
6	3.07	0.032	7.174
7	3.68	0.030	3.174
8	4.30	0.030	0.014

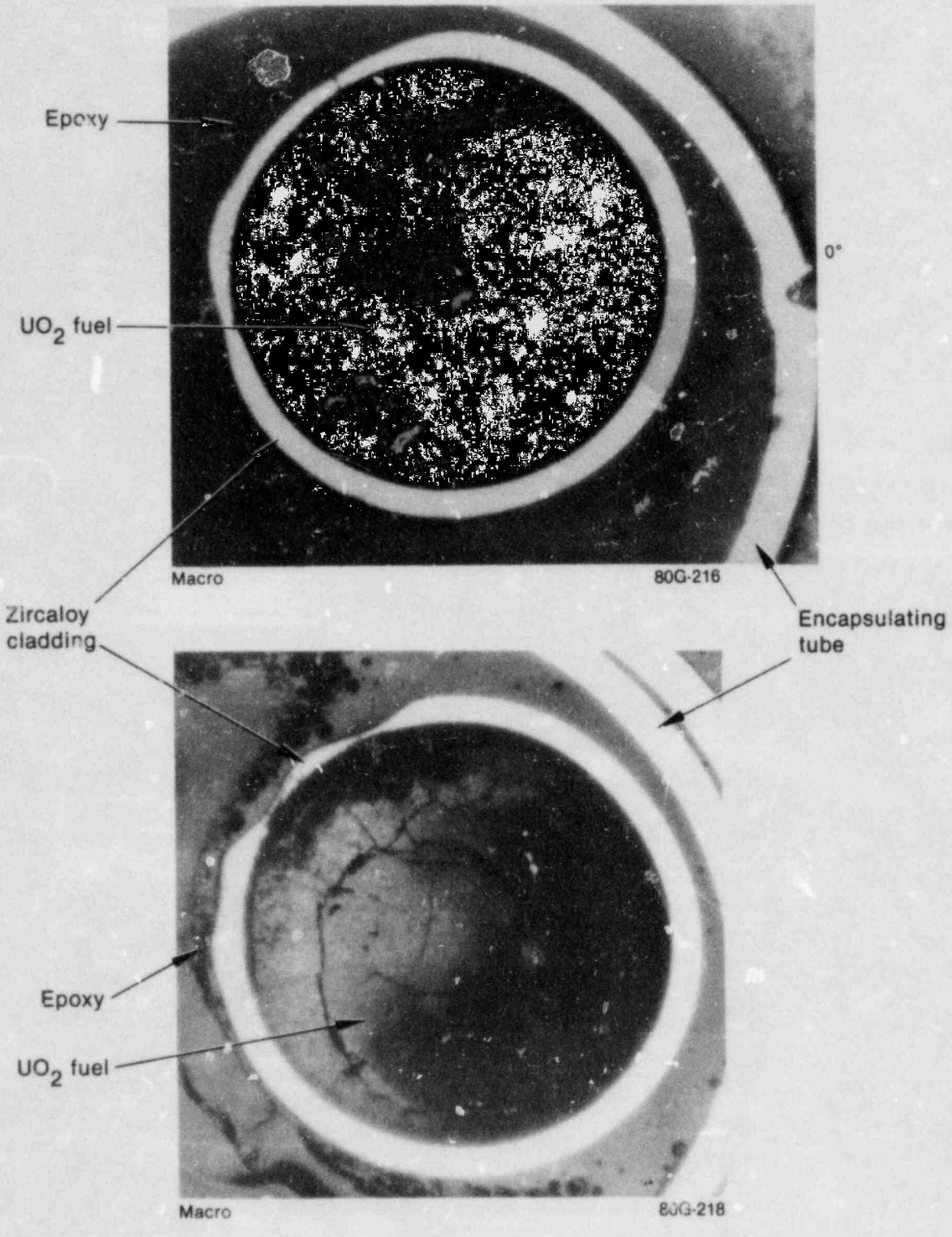

Figure 13. Cross sections of RIA 1-4 rods showing cladding thickening and thinning.

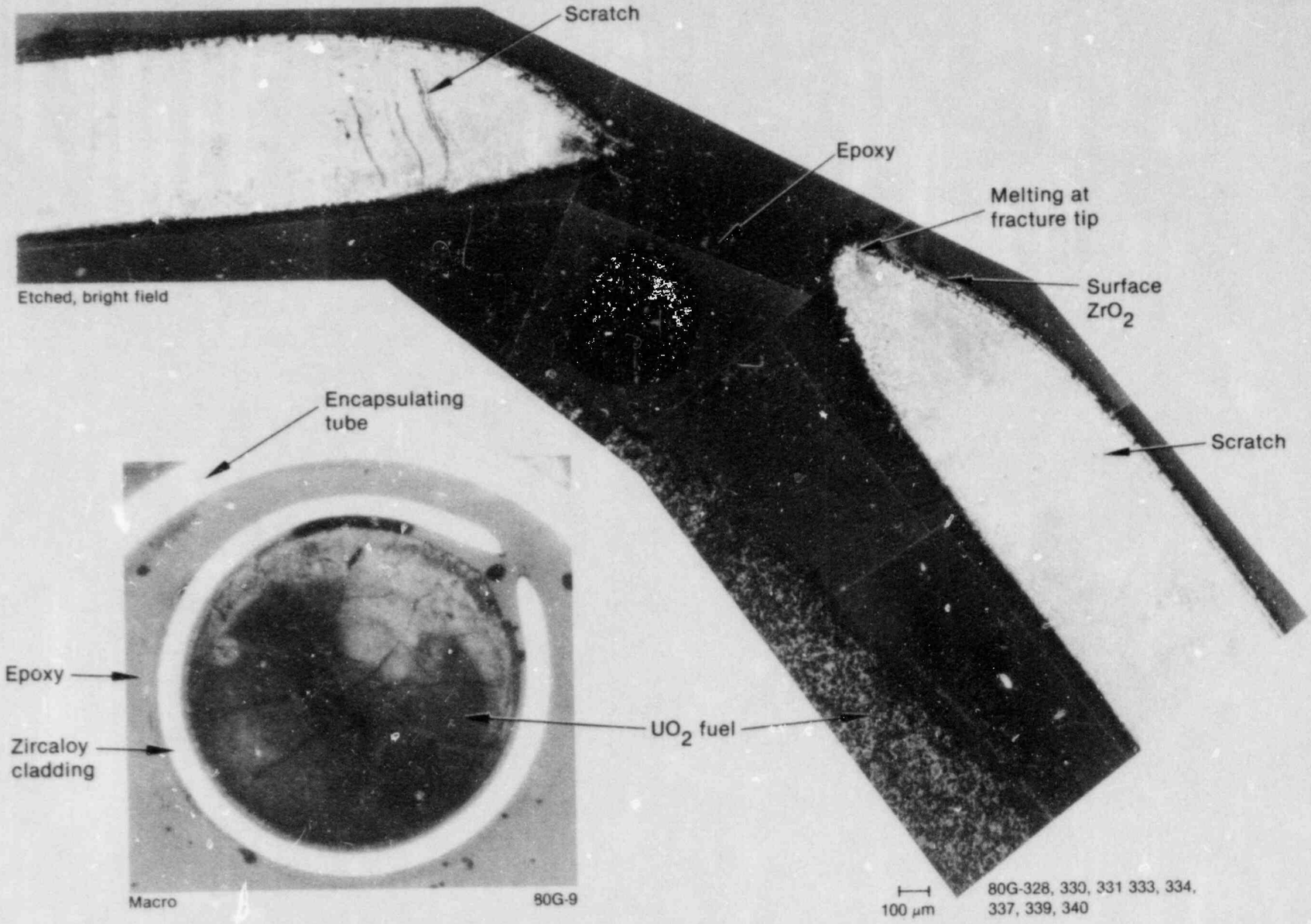

Figure 14. Melting observed at cladding fracture tip; Sample M-64 from Rod 804-6.

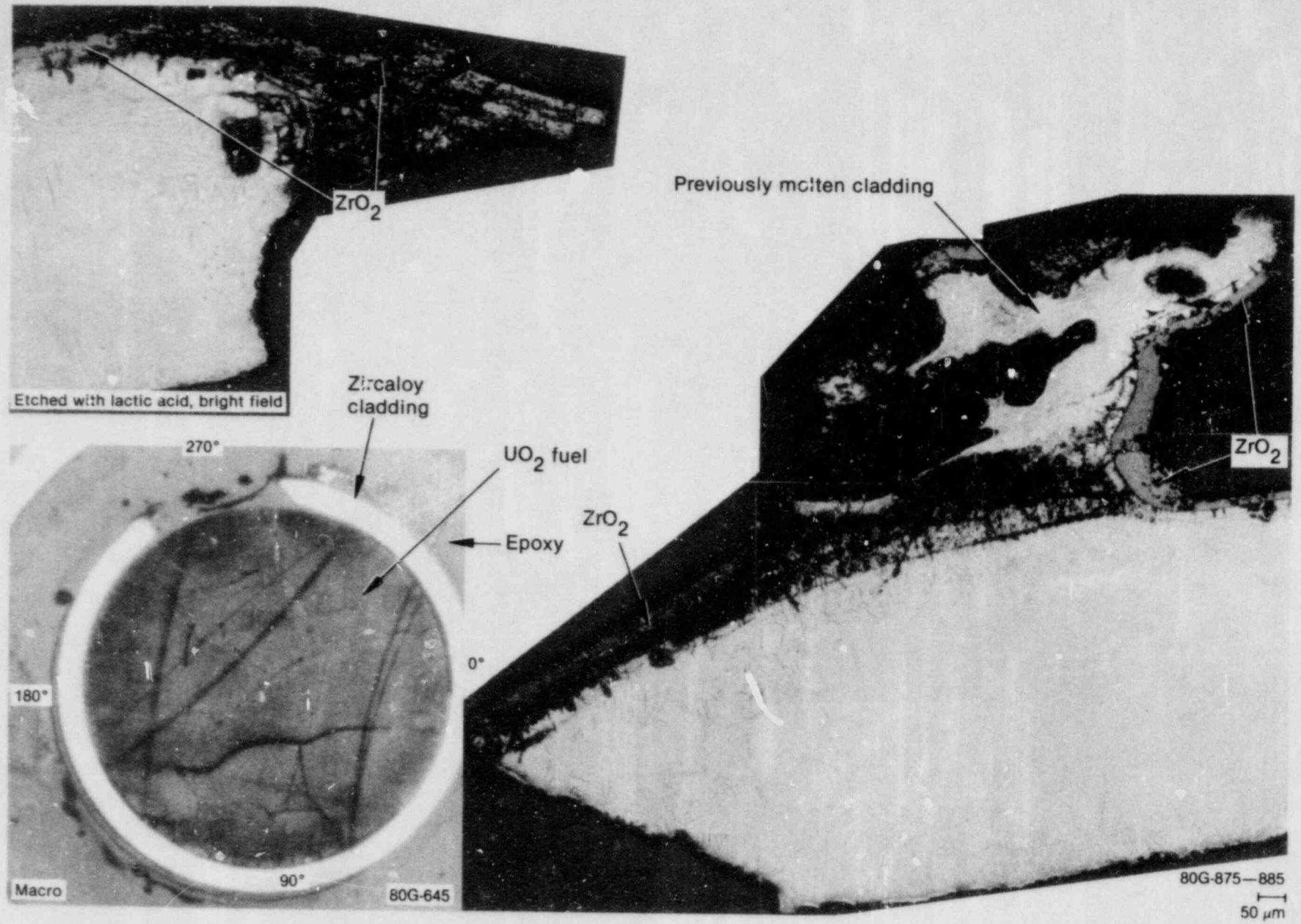

Figure 15. Melting observed at cladding fracture tip; Sample M-52 from Rod 804-5.

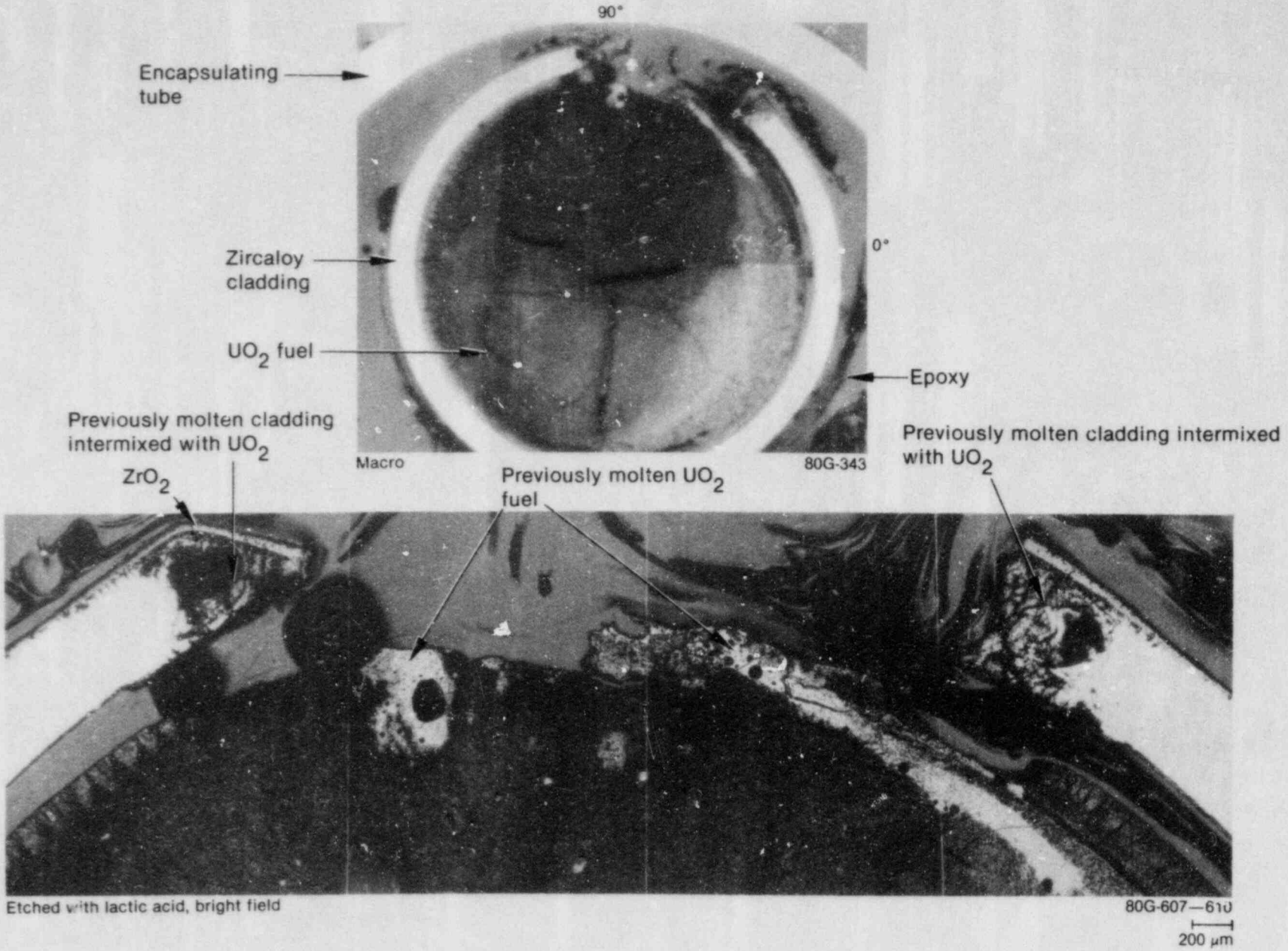

Figure 16. Previously molten fuel and cladding; Sample M-82 from Rod 804-8.

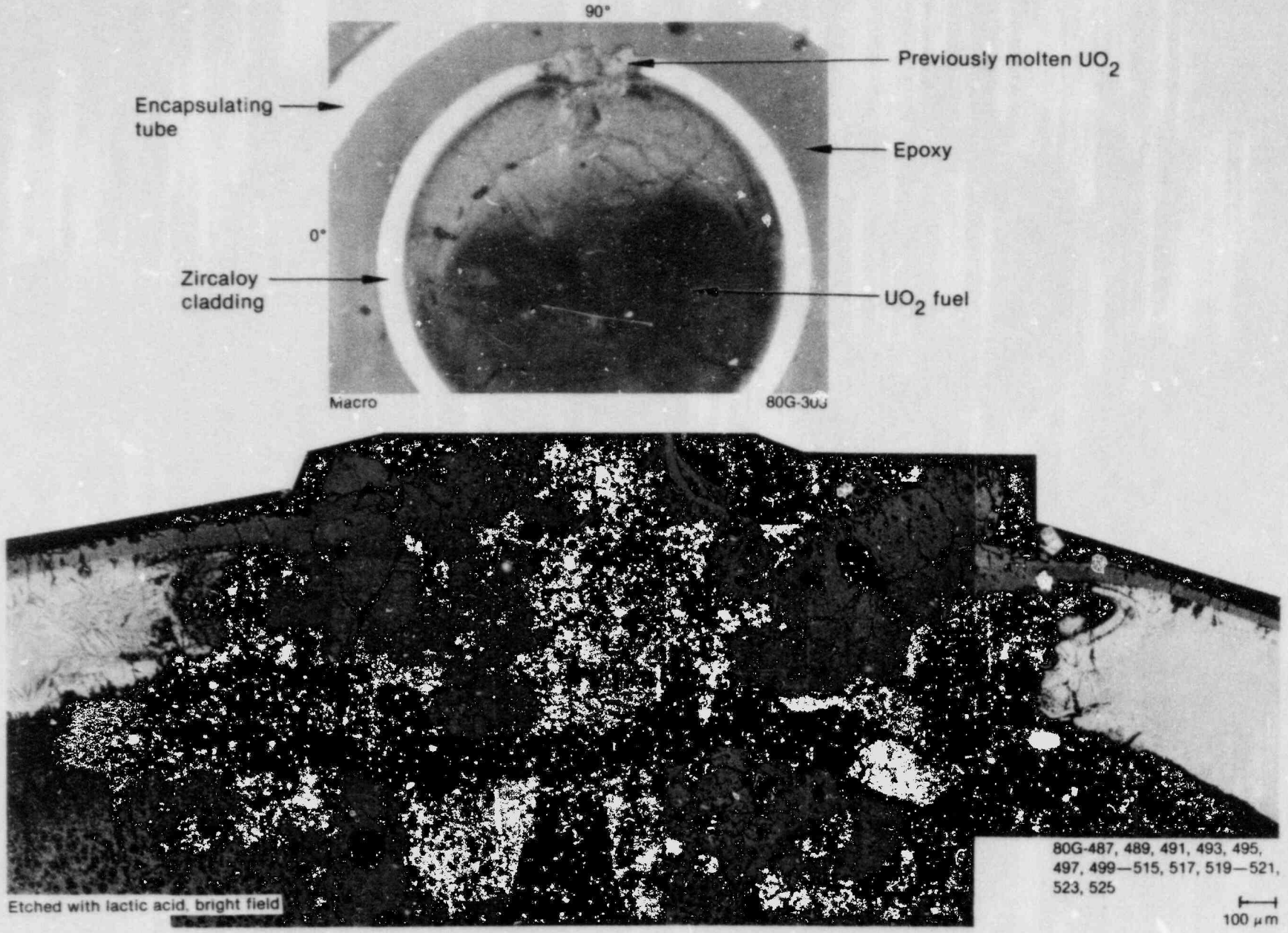

Figure 17. Previously molten fuel and cladding; Sample M-61 from Rod 804-6.

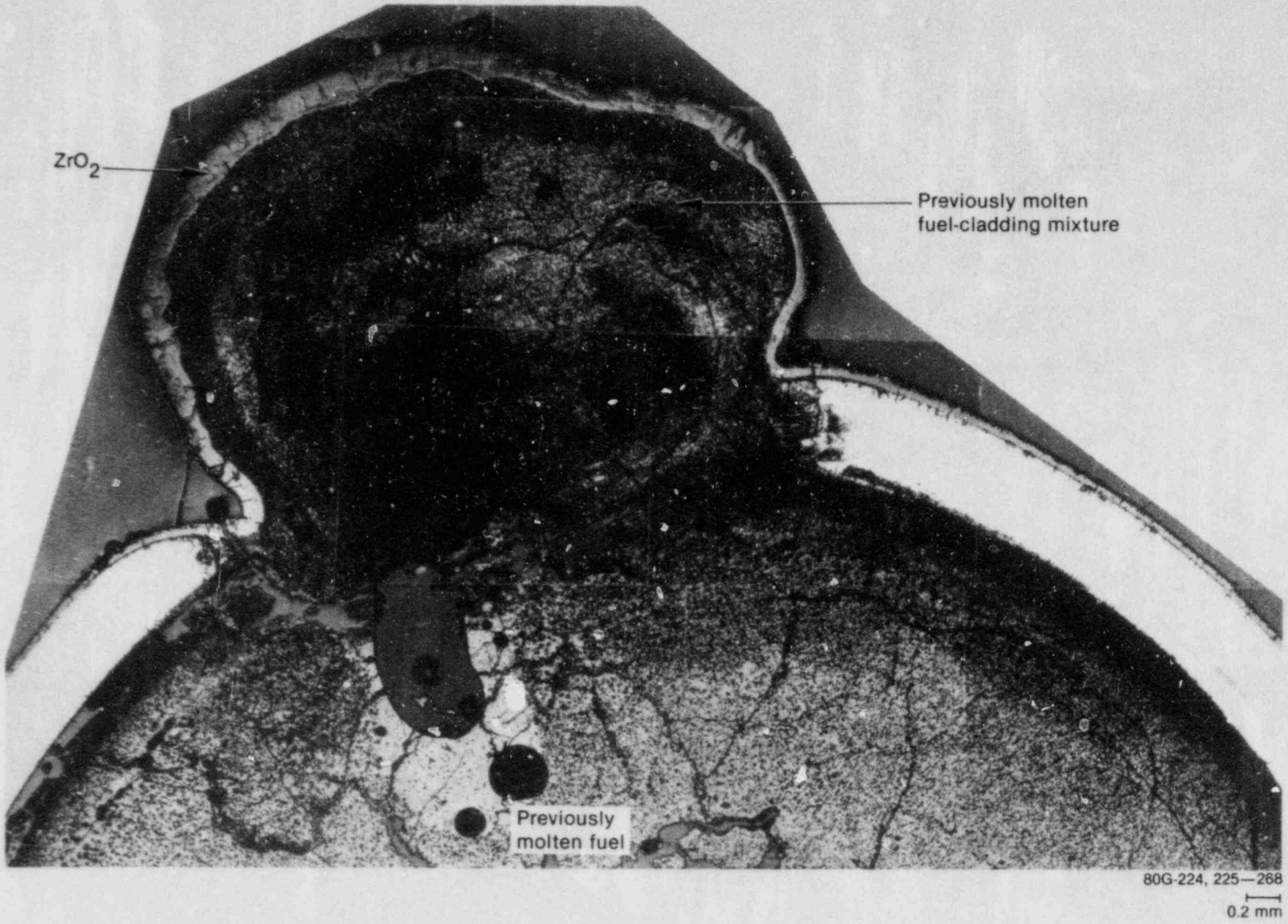

Figure 18. Previously molten fuel and cladding; Sample M-2 from Rod 804-10.

elevation reached melting temperatures. In actuality, there was very little molten fuel in any of the RIA 1-4 rods, and only near the pellet surface. An example showing a typical fuel structure is presented in Figure 19. In general, the fuel microstructure shows the highest fuel temperature close to the surface of the pellet (the radial location of the peak varies slightly from sample to sample). The high temperature gradient at this radial position resulted in a circumferential crack due to the differential thermal expansion of the fuel. On either side of the highest temperature position there is a band of fuel with little restructuring. Although this fuel was probably at high temperature ($\geq$3000 K), it was only at that temperature for a very short time (<1 s). The remainder of the pellet was exposed to high fuel temperatures (less than the fuel melting temperature, however) for between 3 and 13 s.

Fission Gas Movement. The fission process generates the inert gases xenon and krypton at a rate of $\sim$0.3 gas atoms per fissioned uranium atom. Some of this gas is retained in the fuel, either in the fuel matrix or coalesced into gas bubbles resulting in fission gas swelling. The remainder of the gas is released from the fuel into the fuel-cladding gap. Fission gas swelling during an RIA contributes to cladding failure due to overstress by the fuel and foaming of molten fuel.

The amount of fission gas in the fuel matrix increases linearly with burnup until saturation occurs at a low burnup. The higher the fuel temperature, the lower the saturation level, and the sooner saturation is attained. The fission gas in bubbles continues to increase with increasing burnup even after the fuel matrix has reached the saturation level. As the temperature increases, the fission gas bubbles migrate up the temperature gradient, and gas is eventually released from the fuel.[15,16]

The burnup of the RIA 1-4 rods from the previous (Saxton) irradiation was 5300 MWd/tU, and the retained fission gas was in the fuel matrix. The burnup from the PBF transient was on the order of 10^{-5} at. %, so only the effect of temperature and not burnup was important for fission gas movement during the transient.

At low burnup and temperatures below 1373 K, most fission gas remains in the fuel matrix and does not significantly affect the fuel pellet volume. At higher temperatures, the fission gas atoms agglomerate and form fission gas bubbles. An example showing small fission gas bubbles in the fuel matrix is given in Figure 20. Most of the large, angular pores probably formed during fabrication and are not due to bubble coalescence. The higher the fuel temperature, the more mobile are the gas atoms. The fuel temperatures were high enough in Test RIA 1-4 that despite the short time at temperature, considerable bubble coalescence and migration occurred.

When two bubbles collide, coalescence into a single bubble occurs because a single larger bubble has a lower surface energy than that of the two original bubbles. Fission-gas bubble coalescence is significant because an $\sim$40% increase in volume occurs by creating one larger bubble from two smaller bubbles. At a higher temperature, but below the melting point of the fuel, the bubbles are extremely mobile, and coalescence of small bubbles into larger ones results in a large volume expansion of the fuel (fuel swelling). Figure 21 shows a cross section of Rod 804-1. The fuel swelling resulted in a high-strain-rate failure of the cladding and subsequent swelling of the fuel out into the coolant channel.

The gas bubbles move in a random pattern in a solid that is free from temperature gradients and mechanical stress. The bubbles move in a biased direction as a result of a temperature gradient or stress at speeds that depend on the bubble size. The moving bubbles can become trapped at grain boundaries and defects such as dislocations. Figure 22 shows two sections of fuel where the fission gas bubbles have been trapped at the grain boundaries, one in a region where some grain growth has occurred, and the other in a region with no grain growth. When the number and diameters of the grain boundary bubbles are large enough, the bubbles come in contact with one another, and the grain boundary breaks open and forms a continuous network for fission gas release to the fuel-cladding gap. An example of a near-continuous network of fission gas bubbles at the grain boundaries is shown in Figure 23.

Fuel Shattering. Grain boundary fracturing of the fuel (shattering) was observed only in the band of fuel outside the high temperature zone, at the pellet surface. In this region, there was very little grain growth and no coalescence of fission gases into bubbles or migration to the grain boundaries. Analysis of fuel shattering from previous PBF tests indicates that the shattering at grain boundaries only occurs in fuel that has reached temperatures greater than

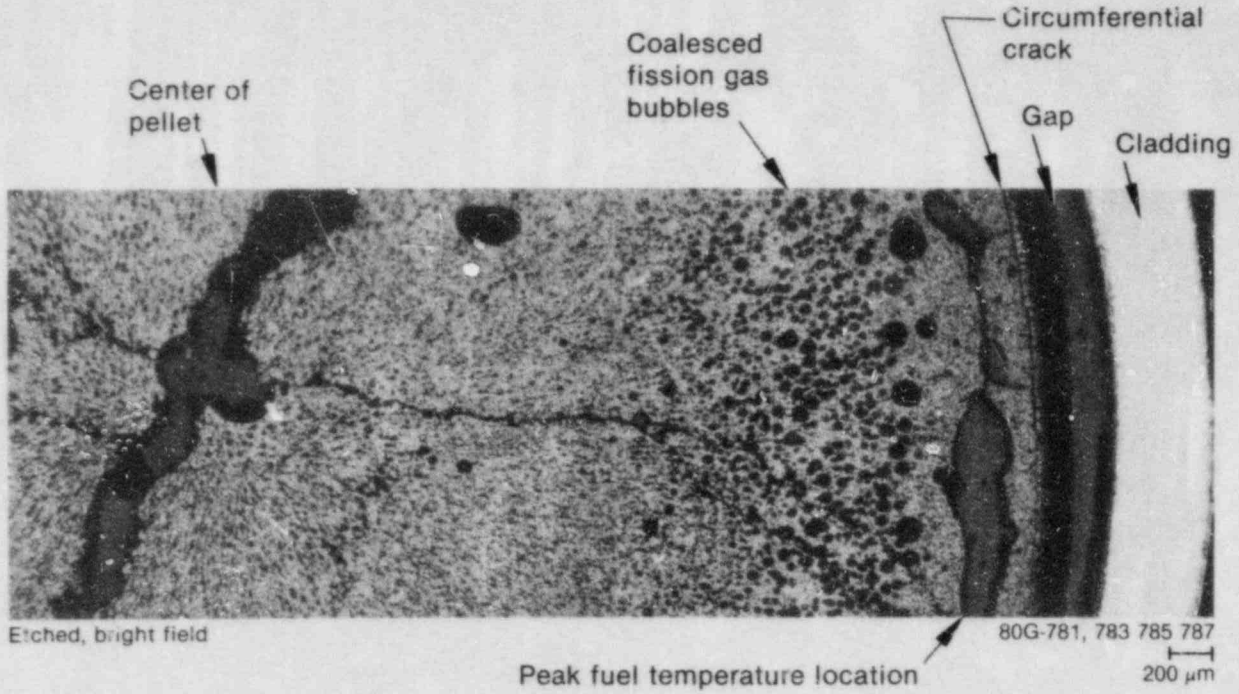

Figure 19. RIA 1-4 typical fuel structure showing location of peak fuel temperature.

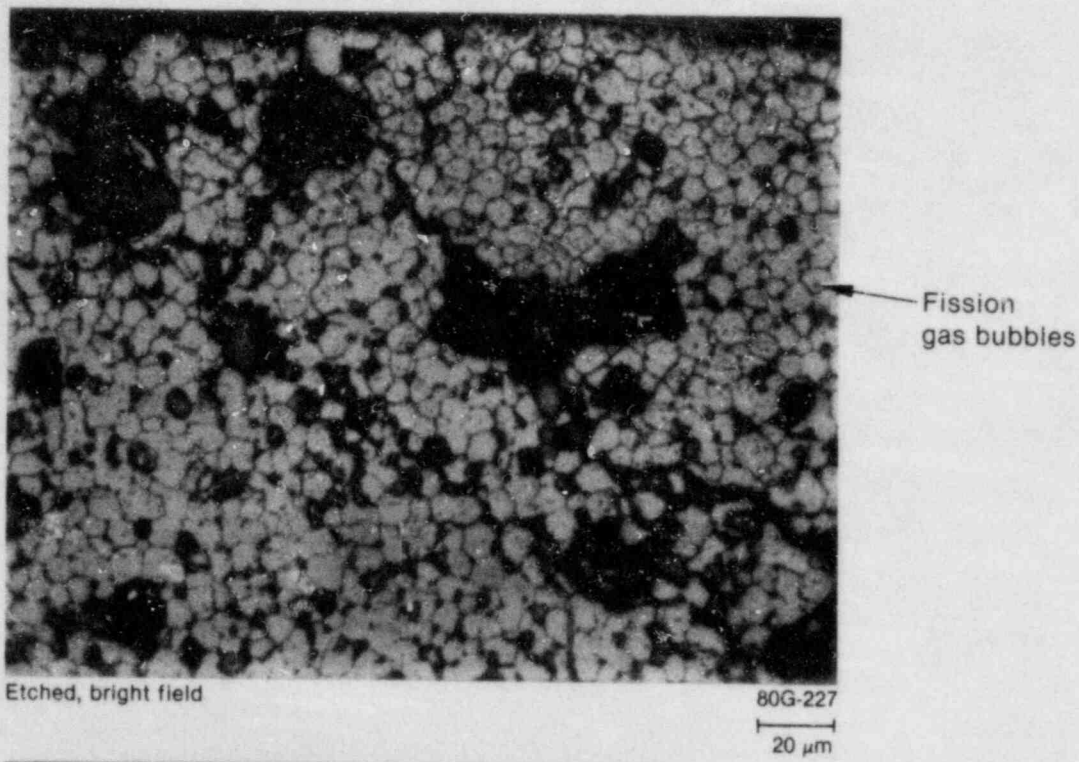

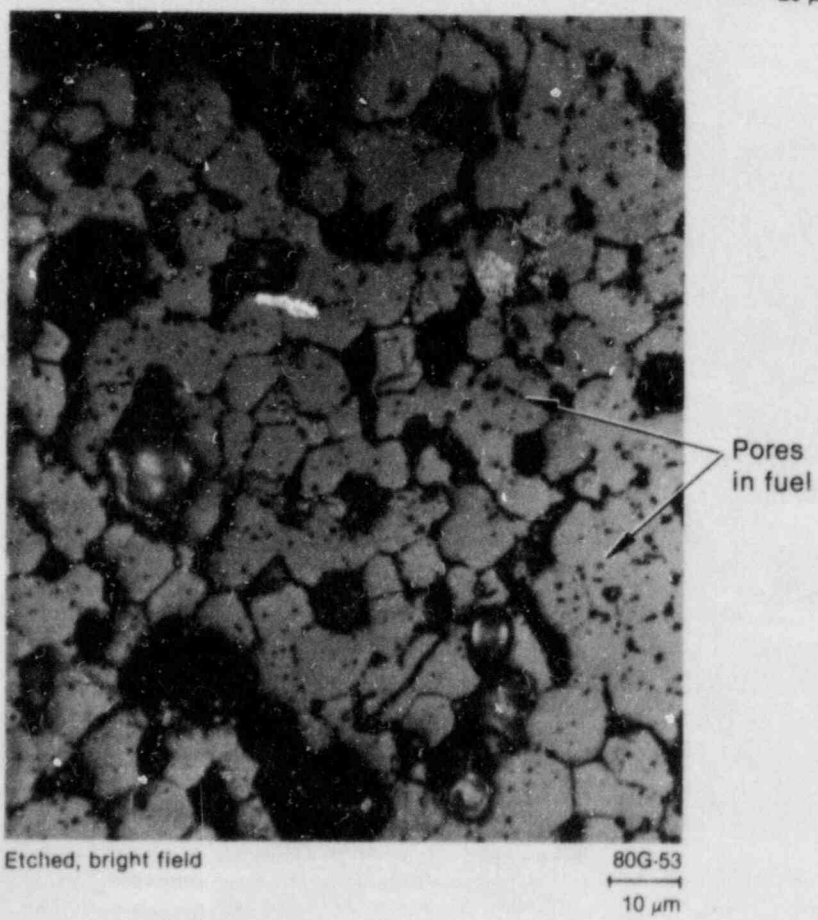

Figure 20. Fission gas bubbles in the fuel matrix.

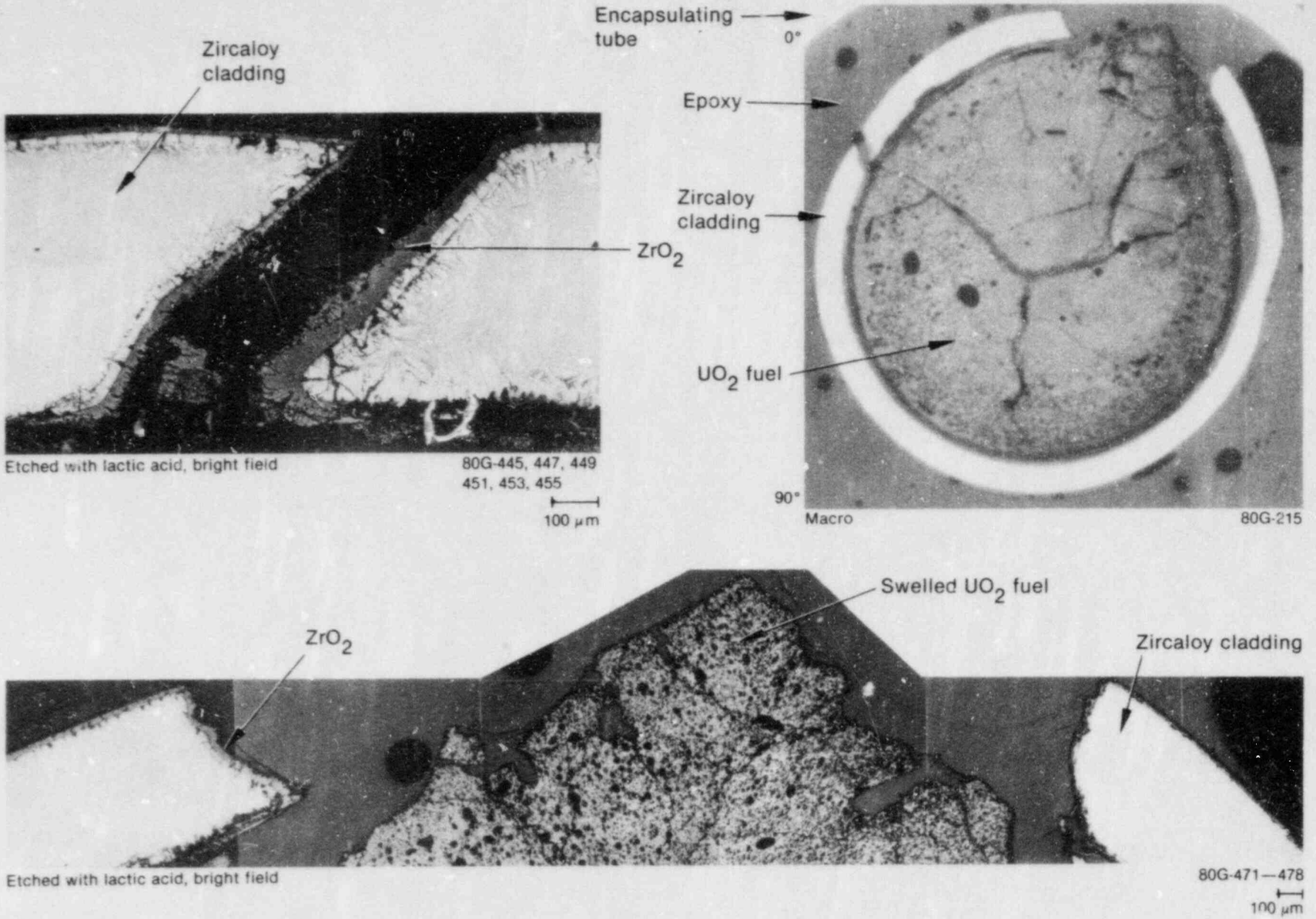

Figure 21. Fuel swelling in RIA 1-4 Rod 804-1.

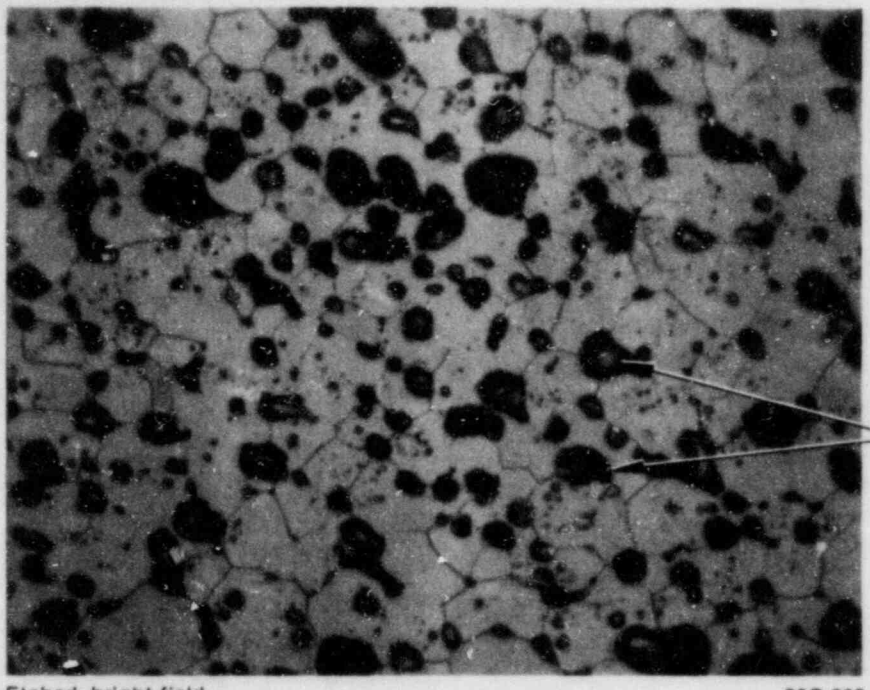

Etched, bright field

80G-228

20 μm

a. Region with grain growth.

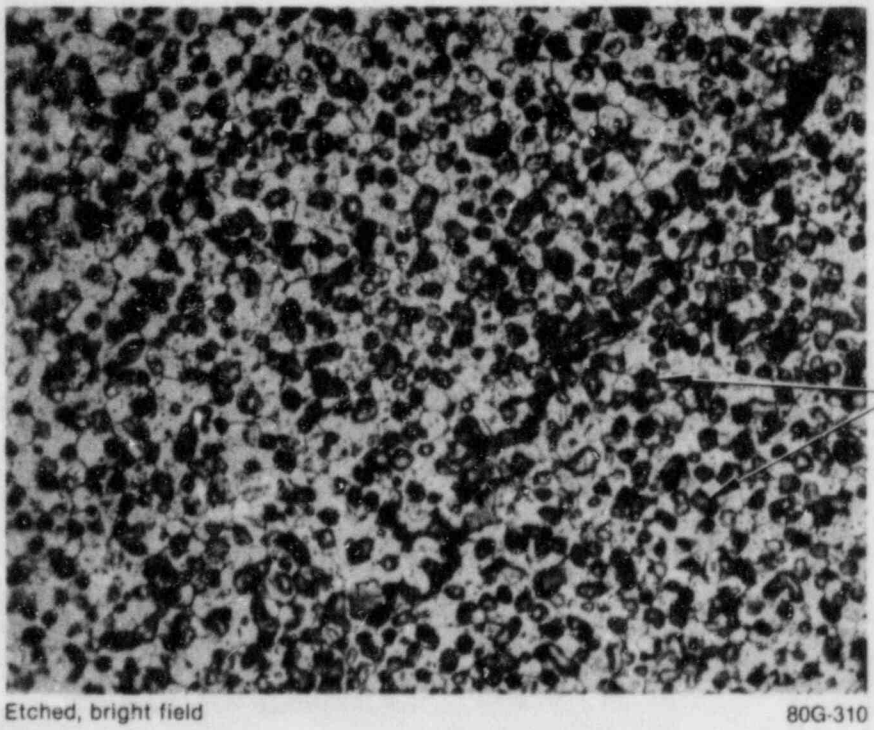

Etched, bright field

80G-310

20 μm

b. Region with no grain growth.

Figure 22. Fission gas bubbles at the fuel grain boundaries

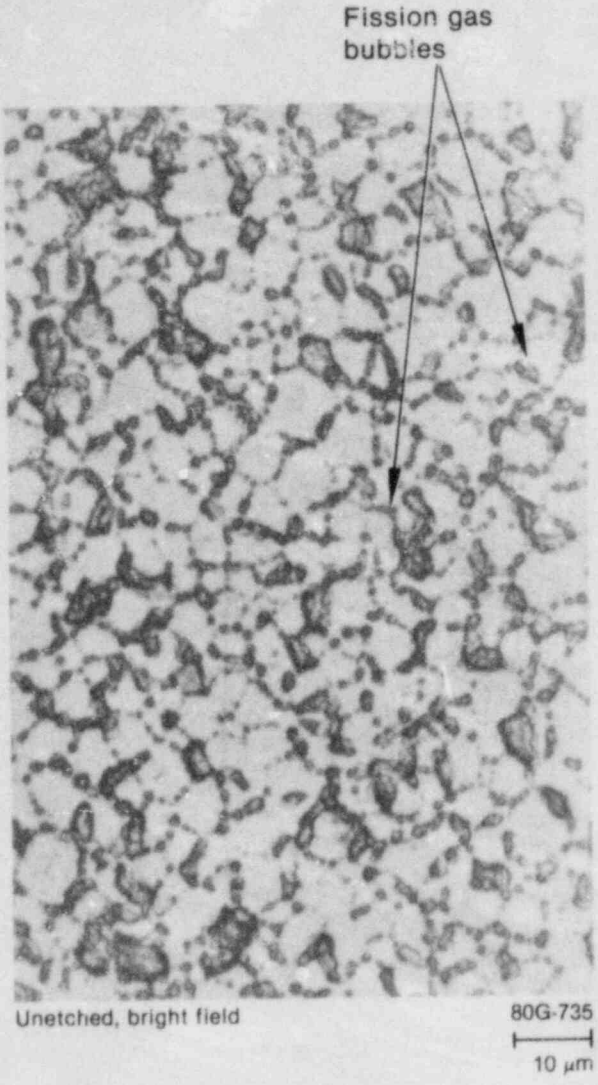

Figure 23. Near-continuous network of fission gas bubbles at fuel grain boundaries.

1900 K, and the shattering occurs on quench.[17] There may be an optimum grain size for shattering to occur, because shattering is not present in fuel with significant grain growth. Because grain boundary fracturing occurs only on quench, it does not substantially affect fuel rod performance during a high temperature transient. Examples of fuel shattering are shown in Figure 24.

Columnar Grain Growth. A narrow (~22-μm wide) region of columnar grain growth was observed near the high temperature region at several elevations. The columnar grains probably formed early in the transient, when this region was at the highest fuel temperature. The columnar grains were formed by preferential pore migration up the temperature gradient for, in this case, a short time. As the location

Figure 24. Fuel shattering in an RIA 1-4 fuel rod.

of the peak temperature in the fuel moved, pores stopped migrating to this location. Because the columnar grain growth region was so small, it did not significantly affect fuel rod performance. Examples of the columnar grain growth are shown in Figure 25.

Fuel Melting. Only limited fuel melting occurred in the RIA 1-4 test rods. The melting occurred in small pockets at the high temperature region near the pellet surface. The molten fuel usually contacted the cladding, because it was close to the fuel surface, and either melted the tips of a previous high-strain-rate failure or resulted in a melt-through failure of the cladding. Examples of fuel melting that resulted in cladding failure are shown in Figures 16 and 17.

Gas bubbles are released when fuel melting occurs. Figure 26 shows a localized area of fuel melting. The melted area is nearly swept clean of fission gas bubbles. The release of gas bubbles from the fuel tends to reduce fuel swelling, but the volume change upon melting tends to increase the swelling.

Fuel Oxidation. Oxidation of the UO_2 fuel can occur when the fuel is exposed to steam for an extended period of time.[18,19] Only one of the locations examined of the nine fuel rods showed any indication of fuel oxidation. Figure 27 shows an overall photograph from the 0.312-m elevation of Rod 804-1 and also a higher magnification photograph of the fuel. The overall photograph shows a uniform color and structure in the fuel; therefore, the higher magnification photograph is representative of all regions in the fuel. The precipitates in the grains in Figure 27b have been identified in other PBF tests as U_4O_9.[18] The U_4O_9 is unstable at temperatures above 1460 K but forms upon cooling. The presence of U_4O_9 at ambient temperatures indicates an O/U ratio in the fuel of between 2.0 and 2.25. The melting point of the fuel is reduced and grain growth is increased with increasing oxygen content.

Samples from Rod 804-1 at elevations 4.1 cm below and 10.7 cm above the location in Figure 27 do not show fuel oxidation. The oxidation seems to be localized to the one elevation of Rod 804-1 and does not appear to have affected fuel rod performance significantly.

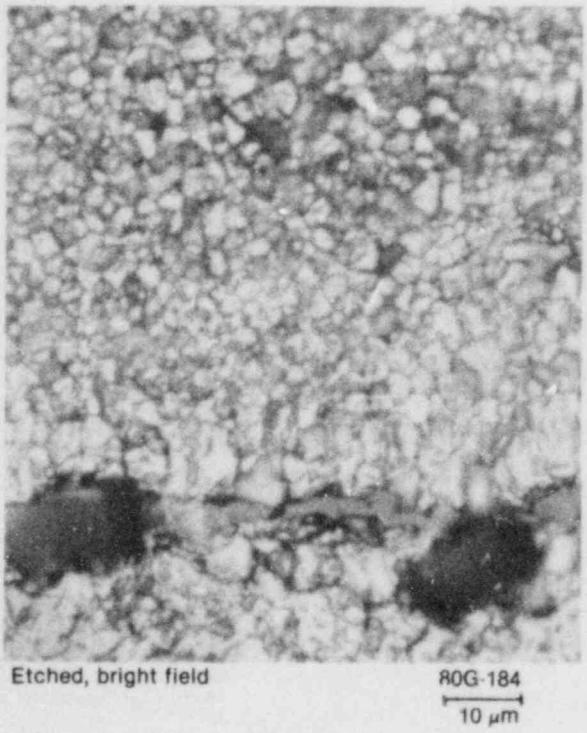

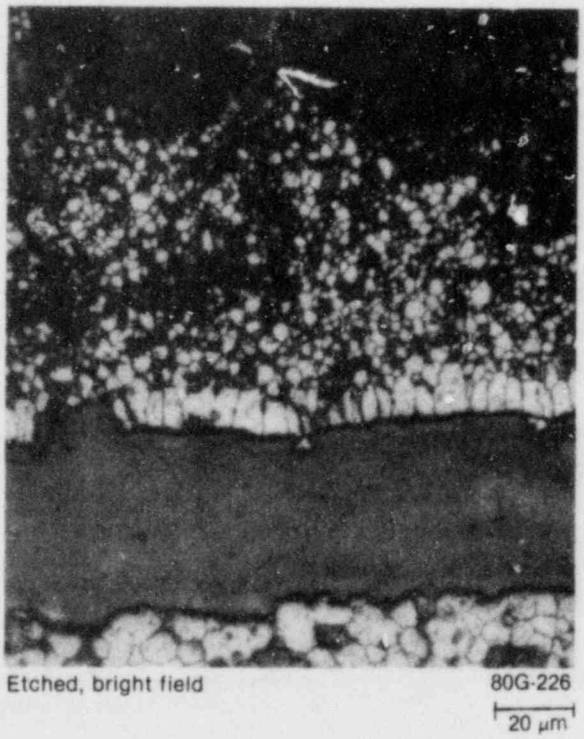

Figure 25. Examples of columnar grain growth near the pellet surface.

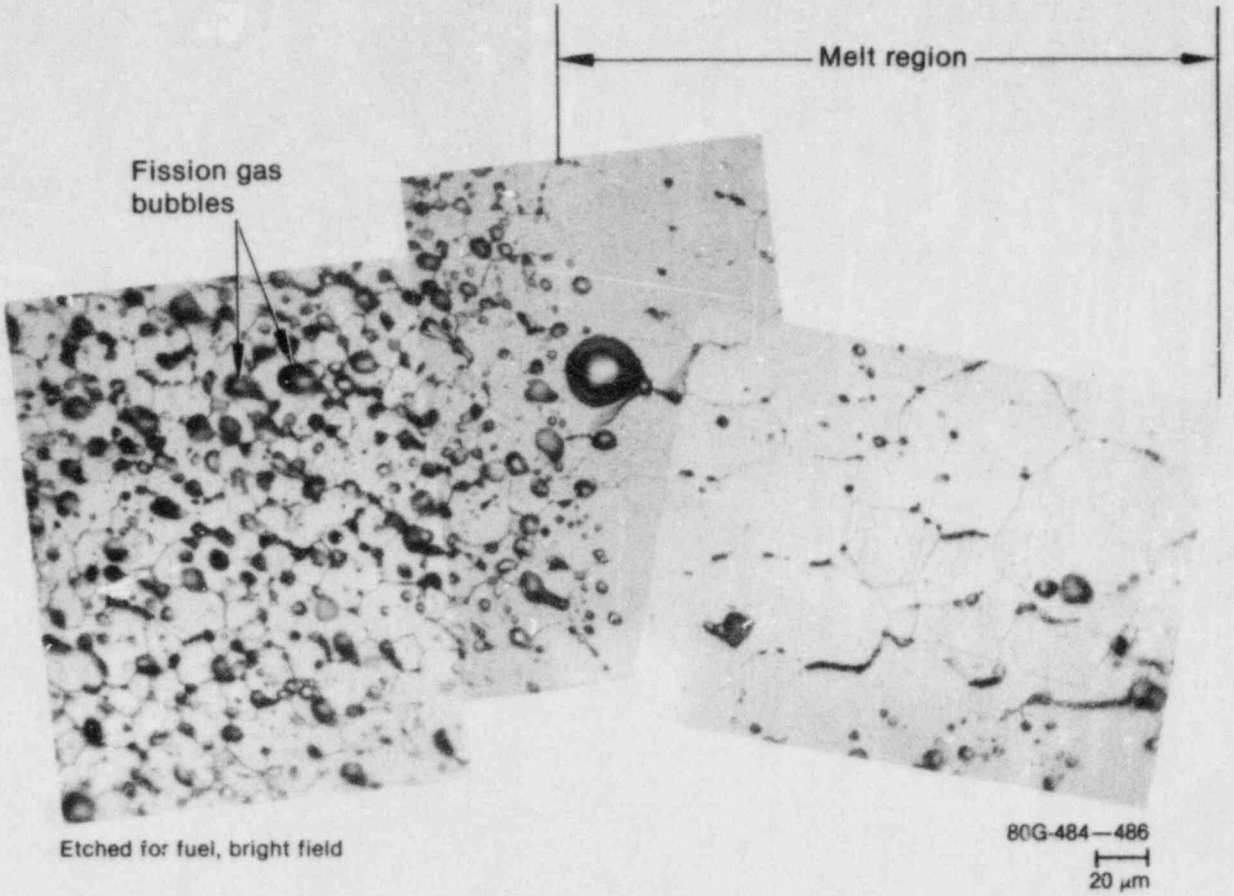

Figure 26. Localized UO_2 fuel melt region nearly swept clean of fission gas bubbles.

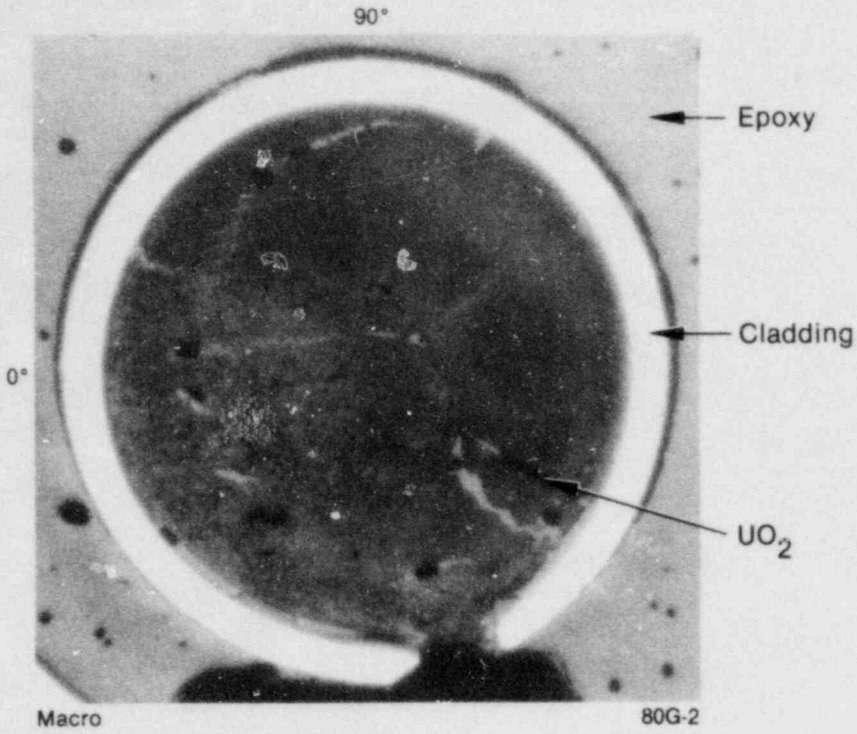

a. Cross section at the 0.312-m elevtion of Rod 804-1.

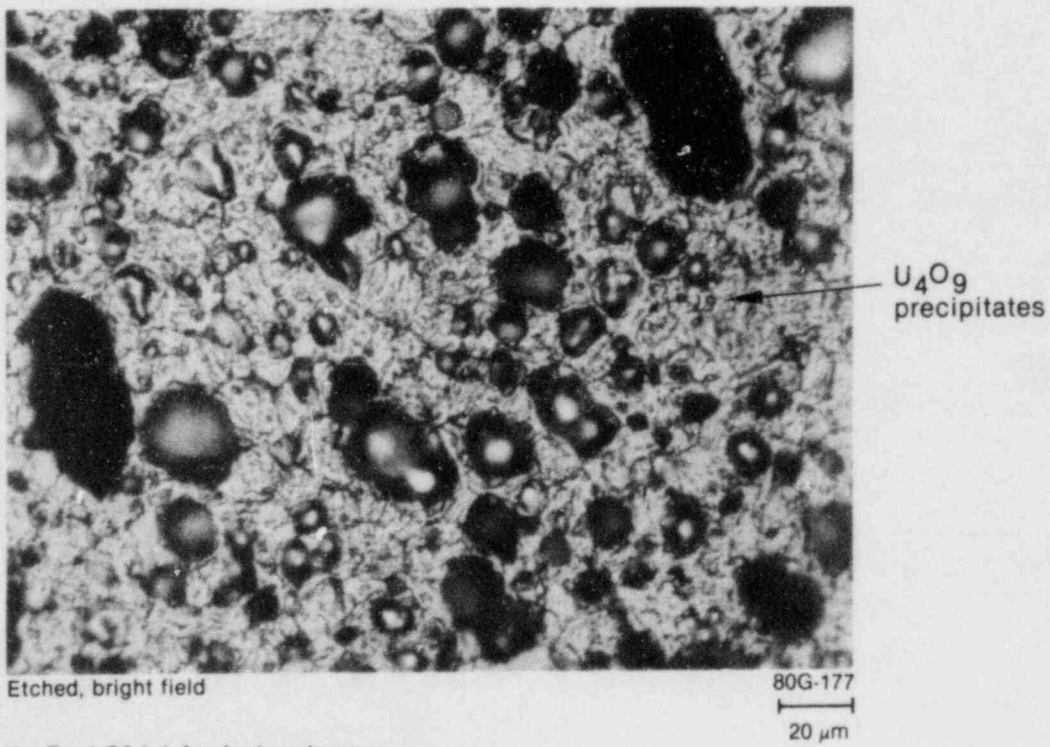

b. Rod 804-1 fuel structure.

Figure 27. Fuel oxidation in RIA 1-4 Rod 804-1.

DISCUSSION

Test RIA 1-4 was conducted to determine fuel rod coolability and channel blockage in a nine-rod cluster during an RIA. Results from the test were to be compared with results from the individually-shrouded fuel rod tests to determine the difference between single-rod and bundle behavior. Comparisons were also to be made between the preirradiated rods in Test RIA 1-4 and previously unirradiated rods tested at the same power levels. Table 6 reviews the PBF RIA Test Series and results from the tests. The corner rods (804-1, -3, -7, and -9) of Test RIA 1-4 operated at about the same radial average peak fuel enthalpy as the Test RIA 1-1 rods. All of the RIA 1-4 rods were bounded in fuel enthalpy by the RIA 1-1 and RIA 1-2 rods. These tests can be used to compare fuel rod behavior in single-rod and bundle tests. RIA-ST-1 and RIA-ST-2 rods were operated at about the same radial average peak fuel enthalpy as the RIA 1-4 side rods but were not preirradiated and can be used to compare preirradiated and previously unirradiated rods. The coolant flow area per rod in the RIA 1-4 test was about 15% larger per rod than for the individually-shrouded rod tests. The initial coolant mass flux was about 9% larger per rod in the bundle test. This change may have affected overall fuel rod performance and will be considered in the comparisons between test rods.

This section discusses differences in rod temperature profile, overall rod condition, and type of failure between single-rod and bundle test rods and preirradiated and previously unirradiated test rods.

Comparison of Single and Bundle Test Rods

Due to neutron flux depression across the bundle, the peripheral rods in the RIA 1-4 bundle showed a circumferential temperature gradient, with the highest temperature occurring on the side of the rod facing the flow shroud. The center rod (Rod 804-5) had a more uniform circumferential temperature distribution, similar to that observed in the single-rod tests. The time in film boiling for the RIA 1-4 rods varied from 6 to 9 s, compared with 9 to 15 s for RIA 1-1 rods and 11 to 18 s for RIA 1-2 rods. The shortened time in film boiling was probably due to the increased coolant mass flux in the bundle test.

There was a significant difference in total damage between the RIA 1-4 fuel rods and the preirradiated single test rods. The final condition of the rods is summarized in Table 6. The RIA 1-4 rods tested at 255 and 277 cal/g UO_2 radial average peak fuel enthalpies exhibited spotty oxide patches, little oxide spalling, small axial splits in the cladding (< 1 cm in length), some small melt-through failures, and no fracturing of the cladding or breakup of the fuel. The center rod, tested at 234 cal/g UO_2, had no axial splits and failed only at locations where molten material from adjacent rods impinged on it. The RIA 1-1 single test rods that were preirradiated showed cladding ruptures, wall thickness variations, heavy cladding oxidation and fragmentation, and fuel and cladding melting. Extensive fuel and cladding fragmentation was observed. Complete blockage of the flow shroud occurred because of fuel swelling and foaming caused by fission gas release at high fuel temperatures. The RIA 1-1 rods had more damage than those rods in Test RIA 1-4, probably because of the extended period of time in film boiling. The peak fuel and cladding temperatures were similar in the two tests, based on the amount of molten fuel and cladding. However, the longer time at high temperature in Test RIA 1-1 resulted in more movement of the molten material, more fission gas coalescence and migration and the resulting fuel swelling and foaming, and more oxidation of the cladding. The difference between the preirradiated bundle test (RIA 1-4) and single-rod test (RIA 1-1) at ~280 cal/g UO_2 was probably due mainly to the difference in coolant mass flux.

The larger coolant mass flux may have reduced the deformation of the cladding and subsequent rod breakup. It has been postulated that cladding wall thinning by plastic deformation may be caused by variations in the local coolant pressure associated with the rapid heating of the coolant during the transient. The larger coolant mass flux in the bundle test probably reduced the local variations in coolant pressure and, therefore, wall thinning in the cladding. The breakup of the rod on quench occurs at regions where the cladding is oxidized all or nearly all the way through. At the power levels in test RIA 1-4 and RIA 1-1, this only occurred in regions of cladding thinning. It is probable that the RIA 1-4 bundle would have shown more of the damage seen in the RIA 1-1 rods had the coolant mass flux been smaller.

Table 6. Results of the PBF RIA Test Series

Test	Rod Number	Burnup (MWd/tU)	Radial Average Peak Fuel Enthalpy (cal/g UO_2)	Comments
RIA-ST-1 Burst 1	ST-1	0	185	Did not fail
RIA-ST-1 Burst 2	ST-1	0	250	Failure; oxidation of cladding, wall thickness variations, cladding embrittlement and fragmentation
RIA-ST-2	ST-2	0	260	Failure; oxidation of cladding, wall thickness variations, cladding embrittlement and fragmentation
RIA-ST-3	ST-3	0	225	Did not fail
RIA-ST-4	ST-4	0	350	Completely destroyed
RIA 1-1	801-1	4600	285	Failure; flow blockage
	801-2	4600	285	Failure; flow blockage
	801-3	0	285	Failure; flow blockage after transient
	801-5	0	285	Failure; flow blockage after transient
RIA 1-2	802-1	5000	185	Did not fail
	802-2	5000	185	Did not fail
	802-3	5000	185	Failure; many high-strain-rate cracks
	802-4	5000	185	Did not fail
RIA 1-4	804-1	5300	277	Failure by high-strain-rate cracks and melt through
	804-3	5300	277	Failure by high-strain-rate cracks and melt through
	804-4	5300	255	Failure by high-strain-rate cracks and melt through
	804-5	5300	234	Failure by molten fuel from adjacent rods
	804-6	5300	255	Failure by high-strain-rate cracks and melt through
	804-7	5300	277	Failure by high-strain-rate cracks and melt through
	804-8	5300	255	Failure by high-strain-rate cracks and melt through
	804-9	5300	277	Failure by high-strain-rate cracks and melt through
	804-10	5300	255	Failure by high-strain-rate cracks and melt through

Comparison of Preirradiated and Previously Unirradiated Test Rods

The previously unirradiated rods subjected to about the same enthalpy as the RIA 1-4 side rods were not instrumented; therefore, times in film boiling could not be determined. The RIA-ST-1 and RIA-ST-2 rods had oxide layers similar in thickness to those observed on the RIA 1-4 rods. However, no fuel or cladding melting was observed in the RIA-ST-1 and RIA-ST-2 rods except for the uranium metal in the fuel-cladding interaction zone. The RIA 1-4 rods showed locations of limited fuel and cladding melting. Therefore, the RIA 1-4 rods operated at higher fuel rod temperatures, but for a shorter time period. The shorter time period was probably due to the increased coolant mass flux. The decrease in fuel conductivity with increasing burnup may have contributed to higher temperatures in preirradiated fuel compared with temperatures in previously unirradiated fuel.

The two previously unirradiated rods subjected to 250 and 260 cal/g UO_2 in Tests RIA-ST-1 and RIA-ST-2, respectively, showed massive oxidation, oxide spalling, cladding splitting and fracturing, wall thickness variations, and fuel and cladding breakup. Approximately 10% of the fuel from the RIA-ST-1 rod and 15% of the fuel from RIA-ST-2 rod passed through 76-μm fuel particle catch screens and into the PBF loop. Gross cladding wall thickening and thinning occurred in the RIA-ST-1 and RIA-ST-2 rods. These rods did not block the coolant flow channel with breakup of the rods.

The temperature ramp rate for the previously unirradiated fuel and cladding was probably similar to that for the preirradiated rods. However, the fuel in the RIA 1-4 side rods swelled more than the fuel in the RIA-ST-1 and RIA-ST-2 rods because of the fission gas and fuel melting. This caused a higher strain rate in the cladding and, consequently, brittle, high-strain-rate failure of the cladding rather than plastic deformation. In Test RIA 1-2, conducted at 185 cal/g with previously irradiated rods, only minimal plastic deformation occurred, and one of the rods failed with 22 brittle, high-strain-rate failures. In Test RIA 1-1, two previously irradiated and two fresh rods were subjected to 285 cal/g. All four rods showed limited melting of the fuel, cladding embrittlement, high-strain-rate failures, plastic deformation of the cladding, and fracture due to through-wall oxidation of thinned cladding regions. It appears that near the failure threshold, the type of rod deformation and failure on the initial power ramp depends on whether the fuel has been previously irradiated; but this effect becomes less significant at higher energy levels.

CONCLUSIONS

This report has presented the analysis and interpretation of the thermal and mechanical response of the Test RIA 1-4 nine-rod bundle. Calculated and observed fuel rod behavior were discussed. This section presents the conclusions from both the RIA 1-4 test and, because this test was the last in the series, the RIA Test Series as a whole.

The PBF RIA Test Series was designed to address the following key safety issues:

- Will there be a loss of coolable core geometry when LWR fuel is subjected to a radial average peak fuel enthalpy of 280 cal/g UO_2?
- Will energetic molten fuel-coolant interactions (vapor explosions) occur during a severe RIA and result in the production of a significant pressure pulse?
- What is the mechanism and threshold enthalpy for failure of LWR fuel during an RIA?

Although only the scoping tests and three of the planned programmatic tests were conducted, data in all of these areas were obtained.

Coolability at 280 cal/g UO_2

Eight fuel rods were tested at radial average peak fuel enthalpies near 280 cal/g UO_2, six of them preirradiated and two previously unirradiated. All of the rods failed. The two preirradiated and two previously unirradiated rods in the single-rod tests lost their rod-like geometries, and their shrouds had flow blockages. The condition of the four preirradiated rods in the corners of the bundle test is not applicable because of the larger flow area. Therefore, based on PBF RIA tests, there may be a loss of coolable core geometry in a LWR if an RIA occurs resulting in a radial average peak fuel enthalpy of 280 cal/g UO_2.

Energetic Molten Fuel-Coolant Interaction

No significant pressure pulse was observed in any of the PBF RIA tests as a result of energetic molten fuel-coolant interactions, except in the case of the RIA-ST-4 test. This test was operated at an energy deposition three times greater than is possible in a commercial reactor during an RIA. A large pressure pulse of 34.6 MPa was measured near the pressure source region, but only low magnitude pressures were measured elsewhere in the in-pile tube and loop piping. Based on these results, vapor explosions do not seem to be a safety concern during an RIA.

Mechanism and Threshold Enthalpy for Failure

Three different levels of fuel rod damage need to be addressed in establishing peak fuel enthalpy limits below which there are no safety concerns as a result of an RIA. Those levels are (a) fuel rod failure threshold, (b) energy deposition that results in loss of rod-like geometry, and (c) energy deposition that results in loss of coolable geometry. It is important to know the initial rod failure threshold for estimating the timing and amount of fission product release to the coolant loop, and subsequent offsite dose consequences. The energy deposition required for loss of rod-like geometry was the most easily determined and correlated data in the PBF RIA Test Series. Breakup of the fuel rods is important to offsite dose consequences and subsequent operation of the core after an RIA. The breakup of the rod is not as dependent on test geometry as is the loss of coolable geometry. Flow blockage during or after an RIA is dependent on the flow channel surrounding the fuel rod. Neither the single-rod, individually-shrouded tests nor the nine-rod bundle test exactly duplicated the flow channels in a commercial LWR fuel bundle.

The failure mechanism for preirradiated and previously unirradiated rods is different. Preirradiated fuel rods failed during heatup, before the rod departed from nucleate boiling, because of the mechanical interaction between the pellet and cladding. This failure occurred at a radial average peak fuel enthalpy as low as 140 cal/g UO_2, although two rods subjected to 185 cal/g UO_2 did not fail. The failure threshold of the previously unirradiated rods was between 225- and 250-cal/g UO_2 radial average peak fuel enthalpy. These failures occurred after the cladding plastically deformed because of the pellet-cladding mechanical interaction, oxidized completely through the wall in the thinned regions, and

quenched. NRC criteria that any rod fails that (a) departs from nucleate boiling in a PWR or (b) is subjected to a radial average peak fuel enthalpy of 170 cal/g or above in a BWR, do not apply to either case. Departure from nucleate boiling is not required for rod failure, and failures can occur at energy depositions as low as 140 cal/g UO_2.

The data from the RIA 1-4 bundle test were not directly applicable in determining the failure threshold for preirradiated rods in a bundle configuration. The rod subjected to 234 cal/g UO_2 failed only because molten material from higher power rods impinged upon it. The rods subjected to 255 cal/g UO_2 failed by high-strain-rate and melt-through failures. Because of the larger coolant flow area, Test RIA 1-4 was not conservative; therefore, in a bundle, the failure threshold would probably be less than 255 cal/g UO_2.

Brittle failure due to mechanical interaction between the pellet and cladding was more prevalent in preirradiated rods than in previously unirradiated rods, near the failure threshold energy deposition. The PBF tests were only conducted with low burnup fuel rods. The failure threshold for high burnup rods by brittle pellet-cladding mechanical interaction failure may be even less.

Although the preirradiated rods had a lower failure threshold than the previously unirradiated rods, the previously unirradiated rods seemed to lose rod-like geometry at a lower fuel enthalpy than the preirradiated rods. This is because of the different failure mechanisms acting near the failure threshold. The previously unirradiated rod subjected to 250 cal/g UO_2 lost rod-like geometry, and the rod at 225 cal/g UO_2 did not. The preirradiated bundle test rods cannot be used to determine a threshold for loss of rod-like geometry, because the large coolant flow area shortened the total time in film boiling and, therefore, the total rod damage. The preirradiated rods subjected to 185 cal/g UO_2 did not lose rod-like geometry. Both types of rods exhibited brittle failure before departure from nucleate boiling and plastic deformation, oxidation, brittle fracture on quench, and loss of rod-like geometry at 285 cal/g UO_2.

Flow blockage in preirradiated rods occurred at 285 cal/g UO_2 radial average peak fuel enthalpy. The blockage was mostly due to foaming of molten, preirradiated fuel. Flow blockage did not occur during the transient in any of the previously unirradiated rod tests even though the rods lost rod-like geometry. After the transient, when the flow was turned off, blockage did occur in the flow shroud of the previously unirradiated rods tested at 285 cal/g UO_2.

REFERENCES

1. United States Nuclear Regulatory Commission, Reactor Safety Program, *A Description of Current and Planned Reactor Safety Research Sponsored by the Nuclear Regulatory Commission's Division of Reactor Safety Research*, NUREG-75/058, June 1975.

2. T. E. Murley et al., "Summary of LWR Safety Research in the U.S.A.," *International Conference on Nuclear Power and Its Fuel Cycle, Salzburg, Austria*, NUREG-0234, May 1977.

3. "Fuel System Design, Section 4.2," *Standard Review Plan for the Review of Safety Analysis Reports for Nuclear Power Plants*, NUREG-75/087, Revision 1 (available from NTIS,UB/B/201-004).

4. *Code of Federal Regulations*, Title 10, Part 50, Appendix A, Criterion 28, "Reactivity Limits."

5. "Assumptions Used for Evaluating a Control Rod Ejection Accident in Westinghouse Pressurized Water Reactors," *NRC Regulatory Guide 1.77*, May 1974.

6. D. H. Risher, Jr., *An Evaluation of the Rod Ejection Accident in Westinghouse Pressurized Water Reactors Using Spatial Kinetics Methods*, WDAP-7588, December 1971, and Revision 1-A, January 1975.

7. C. J. Paone et al., *Rod Drop Accident Analysis for Large Boiling Water Reactors*, NEDO-10527, March 1972.

8. T. Fujishiro et al., *Light Water Reactor Fuel Response During Reactivity Initiated Accident Experiments*, NUREG/CR-0269, TREE 1237, August 1978.

9. P. E. MacDonald et al., "Light Water Reactor Fuel Response During Reactivity Initiated Accident Experiments," *Aspects of Nuclear Reactor Safety*, P. von der Hardt and H. Rottger (eds.), London, England: Harwood Academic Publishers, 1980.

10. S. L. Seiffert, D. E. Owens, S. Shiozawa, "Fuel Rod Behavior During a Reactivity Initiated Accident at Energy Depositions Near 280 cal/g UO_2," *Aspects of Nuclear Reactor Safety*, P. von der Hardt and H. Rottger (eds.), London, England: Harwood Academic Publishers, 1980.

11. P. E. MacDonald et al., "Assessment of Light-Water Fuel Damage During a Reactivity-Initiated Accident," *Nuclear Safety, 21*, No. 5, September-October 1980.

12. R. S. Semken et al., *Reactivity Initiated Accident Test Series, RIA Scoping Tests Fuel Behavior Report*, NUREG/CR-1360, EGG-2024, April 1980.

13. B. A. Cook et al., *Reactivity Initiated Accident Test Series Test RIA 1-2 Fuel Behavior Report*, NUREG/CR-1842, EGG-2073, January 1981.

14. S. L. Seiffert, *Reactivity Initiated Accident Test Series Test RIA 1-1 Fuel Behavior Report*, NUREG/CR-1465, EGG-2040, September 1980.

15. H. Zimmermann, "Fission Gas Behavior in Oxide Fuel Elements of Fast Breeder Reactors," *Nuclear Technology, 28*, 1976, pp. 127-133.

16. D. R. Olander, *Fundamental Aspects of Nuclear Reactor Fuel Elements*, TID-26711-P1, April 1976, pp. 114-118.

17. A. W. Croenberg and T. R. Yackle, "Intergranular Fracture of Unrestructured UO_2 Fuel During Film Boiling Operation," *Journal of Nuclear Materials, 84*, 1979, pp. 295-318.

18. B. A. Cook, *Fuel Rod Material Behavior During Test PCM-1*, NUREG/CR-0757, TREE-1333, June 1979.

19. D. K. Kerwin, *Test PCM-5 Fuel Rod Materials Behavior*, NUREG/CR-1430, EGG-2023, May 1980.

NRC FORM 335 (2-84) NRCM 1102, 3201, 3202

U.S. NUCLEAR REGULATORY COMMISSION

BIBLIOGRAPHIC DATA SHEET

SEE INSTRUCTIONS ON THE REVERSE

1 REPORT NUMBER (Assigned by TIDC add Vol. No., if any)
NUREG/CR-3938
EGG-2336

2 TITLE AND SUBTITLE
Reactivity Initiated Accident Test Series
Test RIA 1-4 Fuel Behavior Report

3 LEAVE BLANK

4 DATE REPORT COMPLETED
MONTH: September
YEAR: 1984

5 AUTHOR(S)
Beverly A. Cook
Zoel R. Martinson

6 DATE REPORT ISSUED
MONTH: September
YEAR: 1984

7 PERFORMING ORGANIZATION NAME AND MAILING ADDRESS (Include Zip Code)
EG&G Idaho, Inc.
Idaho Falls, ID 83415

8 PROJECT/TASK/WORK UNIT NUMBER

9 FIN OR GRANT NUMBER
A6305

10 SPONSORING ORGANIZATION NAME AND MAILING ADDRESS (Include Zip Code)
Division of Accident Evaluation
Office of Nuclear Regulatory Research
U.S. Nuclear Regulatory Commission
Washington, DC 20555

11a TYPE OF REPORT

b PERIOD COVERED (Inclusive dates)

12 SUPPLEMENTARY NOTES

13 ABSTRACT (200 words or less)

This report presents and discusses results from the final test in the Reactivity Initiated Accident (RIA) Test Series, Test RIA 1-4, conducted in the Power Burst Facility (PBF) at the Idaho National Engineering Laboratory. Nine preirradiated fuel rods in a 3 x 3 bundle configuration were subjected to a power burst while at boiling water reactor hot-startup system conditions. The test resulted in estimated axial peak, radial average fuel enthalpies of 234 cal/g UO_2 on the center rod, 255 cal/g UO_2 on the side rods, and 277 cal/g UO_2 on the corner rods. Test RIA 1-4 was conducted to investigate fuel coolability and channel blockage within a bundle of preirradiated rods near the present enthalpy limit of 280 cal/g UO_2 established by the U.S. Nuclear Regulatory Commission. The test design and conduct are described, and the bundle and individual rod thermal and mechanical responses are evaluated. Conclusions from this final test and the entire PBF RIA Test Series are presented.

14 DOCUMENT ANALYSIS - a KEYWORDS/DESCRIPTORS

b IDENTIFIERS/OPEN-ENDED TERMS

15 AVAILABILITY STATEMENT
UNLIMITED

16 SECURITY CLASSIFICATION
(This page) Unclassified
(This report) Unclassified

17 NUMBER OF PAGES

18 PRICE

501

EG&G Idaho, Inc.
P.O. Box 1625
Idaho Falls, Idaho 83415